Journal of Cleaner Production 257 (2020) 120424

Contents lists available at ScienceDirect

Journal of Cleaner Production

journal homepage: www.elsevier.com/locate/jclepro

Examining effects of climate change and land use dynamic on biophysical and economic values of ecosystem services of a natural reserve region

Srikanta Sannigrahi [a, b, *], Qi Zhang [c], P.K. Joshi [d], Paul C. Sutton [e], Saskia Keesstra [f, g], P.S. Roy [h], Francesco Pilla [b], Bidroha Basu [b], Ying Wang [i], Shouvik Jha [j], Saikat Kumar Paul [a], Somnath Sen [a]

[a] Department of Architecture and Regional Planning, Indian Institute of Technology, Kharagpur, 721302, India
[b] School of Architecture, Planning and Environmental Policy, University College Dublin Richview, Clonskeagh, Dublin, D14 E099, Ireland
[c] The Frederick S. Pardee Center for the Study of the Longer Range Future, Boston University, Boston, MA, 02215, USA
[d] School of Environmental Sciences (SES), Jawaharlal Nehru University, New Delhi, 110067, India
[e] Department of Geography and the Environment, University of Denver, 2050 East Iliff, Avenue, Denver, CO, 80208-0710, USA
[f] Soil, Water and Land-use Team, Wageningen University and Research, Droevendaalsesteeg3, 6708PB, Wageningen, Netherlands
[g] Civil, Surveying and Environmental Engineering, The University of Newcastle, Callaghan, 2308, Australia
[h] System Analysis for Climate Smart Agriculture, Innovation Systems for the Dry Lands, ICRISAT, Patancheru, India
[i] School of Public Administration, China University of Geosciences, Wuhan, 430074, China
[j] Indian Centre for Climate and Societal Impacts Research (ICCSIR), Kachchh, Gujarat, 370465, India

ARTICLE INFO

Article history:
Received 1 July 2019
Received in revised form
28 December 2019
Accepted 4 February 2020
Available online 14 February 2020

Handling editor: Richard Wood

Keywords:
Ecosystem services
Climate change
InVEST
CA-Markov
Land use
Sundarbans

ABSTRACT

Ecosystem Service Valuation (ESV) is a process of evaluating and quantifying the monetary values of ESs and their functions. Using both biophysical and spatially explicit integrated models, biophysical and monetary values of key Ecosystem Services (ESs) were estimated in the Sundarbans Biosphere Region (SBR), India. Quantification was made both in time series (1982–2017) and individual years (1973, 1988, 2003, 2013, 2018, 2025, 2035, 2045) to understand the impact of climate change and land-use dynamics on the long-term ecological status of the region. The monetary and biophysical values of the ESs were then obtained from Net Primary Productivity (NPP) models, Integrated Valuation of Ecosystem Services and Trade-offs (InVEST), and Cellular Automata Markov Chain Model (CA-Markov). NPP increased significantly during the first half period (1982–1999), but significantly declined during the second period (2000–2017). The highest estimated ESVs (US$ ha^{-1}) was found for habitat service (30780), nutrient cycling (12626), and gas regulation (7224.81), whereas, lower ESVs were approximated for water regulation (347.81), raw material production (777.82) and waste treatment (13.57) services. Among the nine ESs evaluated, climate regulation, gas regulation, and disturbance regulation were the most important regulating services of the SBR. The combined effects of climate change and land-use dynamics on ESs are much stringent in a vulnerable region like the SBR. Most of the regulating services were closely associated with the fluctuation of land use land cover input. Thus, land management policies and land reform strategies that will encourage the conversion of productive land, especially the highly productive mangrove forest, for the development or any other financial benefits, would disturb the ideal human-nature balance of this ecosystem. The outcomes of this study also provide an important reference to the land administrators, researchers, and decision-makers to comprehend the expected social-ecological juxtaposition in a protected natural reserve region like the Sundarbans.

1. Introduction

Ecosystem services (ESs) are the opportunities and benefits that humans obtain from natural capitals (MA, 2005; Braat and de Groot, 2012; de Groot et al., 2012; Pandeya et al., 2016).

* Corresponding author. School of Architecture, Planning and Environmental Policy, University College Dublin Richview, Clonskeagh, Dublin, D14 E099, Ireland.
E-mail address: srikanta.sannigrahi@ucd.ie (S. Sannigrahi).

https://doi.org/10.1016/j.jclepro.2020.120424
0959-6526/

Ecosystem service values (ESVs) are quantified estimates of natural goods and services (Johnston and Russell, 2011), which indicate economic significance (Sannigrahi et al., 2018, 2019a,b) as well as the status and health of an ecosystem (Peng et al., 2015; Costanza, 2012; Yan et al., 2016). Several direct and indirect factors are responsible for the destabilization of ESs (Chen et al., 2019; Wu et al., 2019; Marx et al., 2019; Sahle et al., 2019). These factors include biophysical dynamics (e.g., changes in climatic conditions, soil properties, plant functional structure, ecological compositions, and structures) and anthropogenic activities (e.g., land degradation, land use change) (Lü et al., 2012; Hauck et al., 2013; Zoderer et al., 2016; Langerwisch et al., 2017; Wang et al., 2018; Zhang et al., 2018, 2019). However, identification of these factors and as well as the estimation of their relative contributions to the degradation of ESs is challenging (Marx et al., 2019; Sannigrahi et al., 2020).

The green capital, derived from many natural goods and services, provides an opportunity for measuring the substantial impact of empowering human development and socio-economic welfare (MA, 2005; Costanza et al., 2014, 2017). However, little effort has been made so far to explore these aspects. The Millennium Ecosystem Assessment (MA, 2005) found that 60% of the ESs and natural goods are under threat due to the exploitation of natural resources by humans. Therefore, proper monetary evaluation is essential to assess the aspects related to the violation of ESs (Liu et al., 2019b; Watson et al., 2019). Consistent and timely ESs assessment can be an alternative for measuring the status and health of an ecosystem (Yu and Han, 2016; Peng et al., 2015; Costanza, 2012). Therefore, in this study, an effort has been made to evaluate the status of a natural reserve region through the spatially explicit valuation of ecosystem services.

The interaction among ESs can be categorized into two types – positive (synergy) and negative (trade-off), depending on the types of ESs taken into consideration (Cademus et al., 2014; Sannigrahi et al., 2019a). Synergy refers to the unidirectional change of two ESs and exhibits a win-win situation that involves a shared increase of two ESs (Tomscha and Gergel, 2016). Whereas, trade-offs refer to a win-lose or lose-win situation when the supply inputs in gaining one ES would reduce another ES (Rodríguez et al., 2006; Wang et al., 2019). Amongst the four interaction groups of ESs, trade-offs often occur between the provisioning and regulating services (Bennett et al., 2009; Haase et al., 2012; Li and Wang, 2018).

The spatial trade-off and synergy are apparent when prioritization of one group of ESs leads to a restriction of another group of ESs, happening especially in inter-regional ES assessment (Liu et al., 2018; Li et al., 2018). For instance, forest degradation in a hilly region for road construction can cause a long term decline of regulating services such as freshwater supply, climate regulation and erosion control in another region (Luo et al., 2018). The temporal trade-off explains that the current uses of ESs of a given region influence the future changes of the same ESs under different management scenarios (Liu et al., 2018). For example, the excessive use of chemical fertilizers and pesticides for increasing food grain can manifest a negative impact on water quality, habitat provision, biodiversity, and/or soil formation in future time. Finally, the term spatial and temporal synergy refers to the unidirectional increases of multiple ESs that happen both spatially and temporarily (Yang et al., 2018; Luo et al., 2018).

In this study, ecosystem service values in the Sundarban Biosphere Region (SBR) were quantified using different valuation approaches. The quantification utilized a set of approaches including Integrated Valuation of Ecosystem Services and Trade-offs (InVEST) biophysical models, replacement cost, damage cost, mitigation cost, direct benefit transfer, market-based valuation, and expert-based valuation. The SBR was selected as the study region because of its highly important landscape with the biodiversity and ecological significance. Despite the profound significance in delivering multiple key ecosystem services for sustaining human well-being and improving the overall socio-ecological status of the region, only a few studies have evaluated the economic suitability of this ecosystem (Everard et al., 2019; DasGupta et al., 2019). The present study is carried out for different single reference years, i.e., 1973, 1988, 2003, 2013, and 2018, for a time-lagged assessment of ecosystem services. In addition, a continuous time-series assessment from 1982 to 2017 was also performed to assess the impact of climate change and land degradation on ecosystem services in the SBR. Several other aspects, including the time-lagged and spatio-temporal assessment of trade-offs and synergies, the cellular automata Markov chain (CA-Markov) model with future prediction of land use and land cover (LULC) for assessing the impact of landscape changes on ESs, conservation priority zonation and ecosystem service hotspot assessment, were integrated to describe the overall socio-ecological status of the region and its linkages with the provision of ecosystem services. Specific objectives of this study are (1) quantifying the monetary values of different ESs using InVEST and other valuation approaches; (2) estimating future LULC changes and their effects on ESs; (3) investigating time-lagged and spatial trade-offs and synergies between ESs to measure the impact of management factors on ESs.

2. Materials and methods

2.1. Study area

The Sundarbans Biosphere Region (SBR) is a highly productive region, earning itself as one of the biodiversity hotspots in the world. The Sundarbans mangrove is the largest single tract mangrove forest in the world with an aerial extent of 10,000 km^2, among which India and Bangladesh share 40% and 60%, respectively (Giri et al., 2011). The SBR ecosystem is of critical importance for its profound biological and ecological values. Several biodiversity and environmental protection measures have been initiated under the scheme of the National Man and Biosphere Programme to preserve the ecological stability of this region. The landward limits of this region are demarcated by the Dampier-Hodges line. The SBR consists of several eco-sensitive areas including the Sundarbans National Park (SNP), Sundarban Tiger Reserve, Wildlife Sanctuaries, i.e., Sajnekhali, Haliday Island, and the Lothian Island (Fig. 1). Additionally, the entire SBR is sub-divided into several distinct eco-regions including the core zone (1700 km^2), a buffer zone (2400 km^2), restoration zone (230 km^2) and development zone (5300 km^2) (Nandy and Kushwaha, 2011). The increasing physical (sea level rising, coastal erosion, flood, storm surge) and socio-economic (environmental migration, economic instability, lack of livelihood options) threats apparent in the Sundarbans, especially in the last decades, seek thorough socio-ecological analysis to explore the economic importance of the Sundarbans. The mangrove ecosystems of the Sundarbans are highly beneficial for protecting coastal biotic and abiotic communities from seawater intrusion, flood, storm surges wind/tide/wave actions and providing many provisioning services such as fishing, food production, honey collection, forestry products. Additionally, among the 50 true mangrove plant species documented throughout the world, the Sundarbans (considering both Indian and Bangladesh share) alone comprise 35 species, which earmarks the great significance of this vibrant and pristine ecosystem (Rahman and Asaduzzaman, 2013).

2.2. Data preparation and analysis

In this study, 16-day time series of 30m spatial resolution

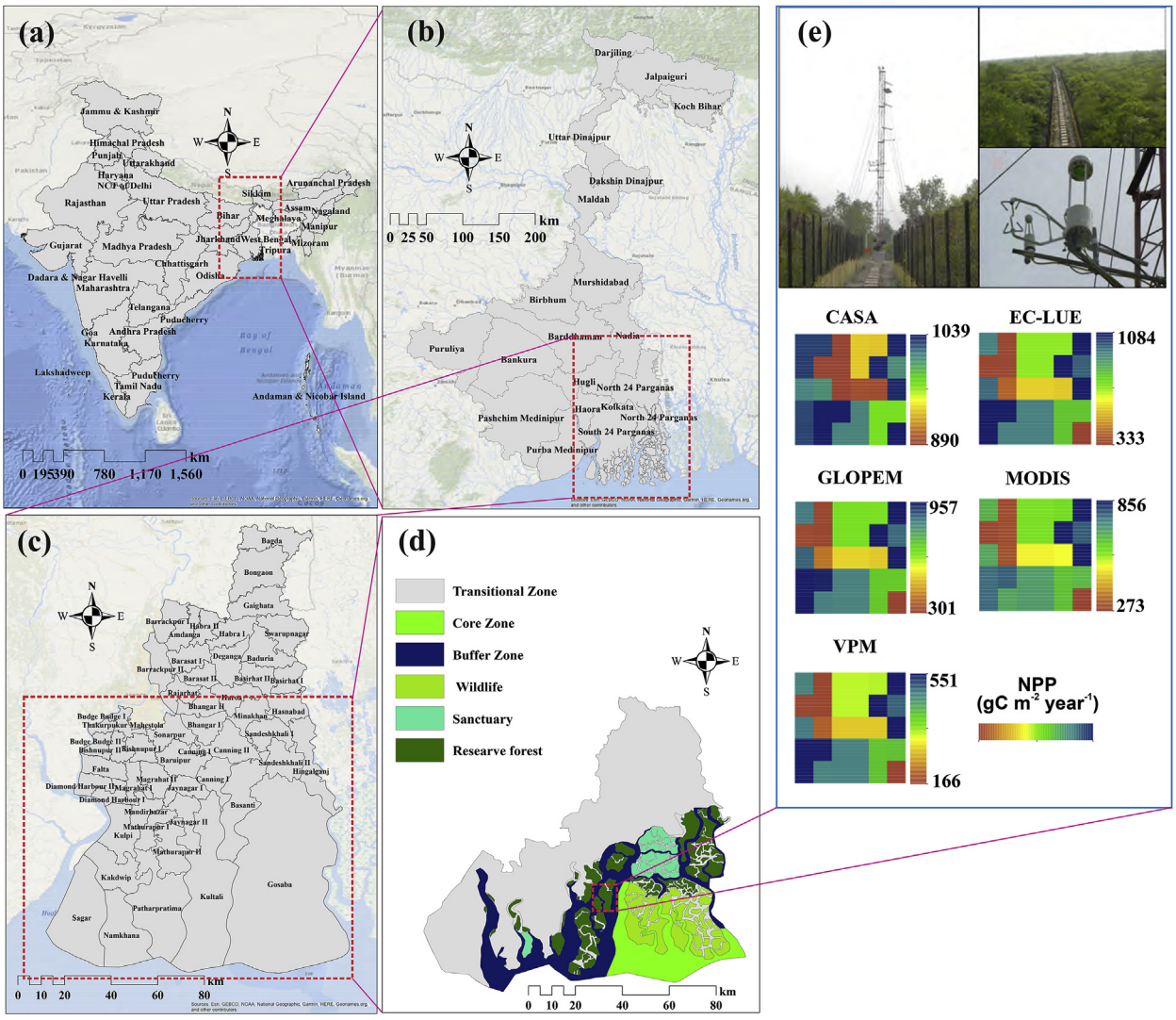

Fig. 1. (a), (b), (c), (d) Location of the study region, (e) location of Sundarban flux tower (After Rodda et al., 2016) and NPP derived from five ecosystem models.

Landsat Multispectral Scanner (MSS), Thematic Mapper (TM), Enhanced Thematic Mapper (ETM), and Landsat Operational Land Imager (OLI) and Thermal Infrared Sensor (TIRS) data products were utilized to classify the SBR into several land use and land cover (LULC) units. Landsat Tier 1 data products, which have the maximum available data quality (Liu et al., 2019a; Qiu et al., 2019), were used for time-series LULC analysis. The Landsat Tier 1 data collection comprises Level-1 Precision and Terrain (L1TP), which exhibits a negligible geometric error (≦ 12m radial root mean square error) and a high image-to-image tolerance approximation (https://www.usgs.gov) (Storey et al., 2014; Dwyer et al., 2018). Additionally, smoothed and filtered MOD13Q1 16 day composite 250m time series Enhanced Vegetation Index (EVI) and Normalized Difference Index (NDVI) datasets for 2000–2017 were retrieved from the University of Natural Resources and Life Sciences, Vienna (https://search.earthdata.nasa.gov/search?q=MOD13Q1%2520V006). For the earlier period (1982–1999), the advanced very high-resolution radiometer (AVHRR) NDVI data were also utilized for the estimation of net primary productivity (NPP) and ecosystem services (ESs). Using the ArcPy python package module (https://www.esri.com/en-us/home), 16-day MOD13Q1 NDVI/EVI scenes was aggregated into the yearly unit for the final calculation.

The required climatic data layers, including maximum, minimum and average temperature (°C), precipitation (mm), latent heat (W m^{-2} s^{-1}), sensible heat (W m^{-2} s^{-1}), incoming solar radiation (W m^{-2}), actual and potential evapotranspiration (mm), surface runoff (mm), soil moisture (mm), vapor pressure (kPa), vapor pressure deficit (kPa), and climate water deficit (mm), were retrieved from TerraClimate (http://www.climatologylab.org/terraclimate.html). The detail description of these data layers is given in Table 1.

The carbon pool information for the InVEST carbon model is derived from the published literature (Liang et al., 2017; Sil et al., 2017; Clerici et al., 2019). The soil data layers including root depth, plant available water content, soil texture, and soil organic carbon were derived from the Food and Agriculture Organization Harmonized World Soil Database v1.2 (http://www.fao.org/soils-portal/soil-survey/soil-maps-and-databases/harmonized-world-soil-database-v12/en/) and National Bureau of Soil Survey and Land Use Planning (NBSS&LUP, Govt. of India) (https://nbsslup.in/). The topographic variables, including elevation and slope, were derived from 90m Shuttle Radar Topography Mission (SRTM) data (http://srtm.csi.cgiar.org/). Development indicators including road layers, location of the urban and residential centers, were derived from the

Table 1
Description of data layers used in this study.

Data layer	Source	Description	Spatial Resolution	Temporal Resolution
MOD13Q1	https://search.earthdata.nasa.gov/search?q=MOD13Q1%2520V006, http://ivfl-info.boku.ac.at/	Smoothed EVI and NDVI data	250m	16 days
AVHRR		Normalized Difference Vegetation Index-3rd generation (NDVI) using the	1/12°	Daily
GIMMS	https://ecocast.arc.nasa.gov/data/pub/gimms/	Global Inventory Monitoring and Modeling System (GIMMS).		
Climate data	http://www.climatologylab.org/terraclimate.html	Climatic layers, including Maximum, minimum, average, and optimum	0.05°	Monthly
	https://esgf-node.llnl.gov/search/cmip5/	temperature, precipitation, solar radiation, actual and potential	0.5625 *	Daily/
Future Climate Data	https://www.worldclim.org/cmip5_30s	evapotranspiration, runoff, soil moisture, vapor pressure, and vapor pressure deficit	0.55691342 1 km	yearly Monthly
		Model for Interdisciplinary Research on Climate (MIROC) Representative Concentration Pathway (RCP) 4.5 precipitation, temperature data for 2025 and 2035		
		Hadley Global Environment Model 2 WorldClim temperature and precipitation data for 2045		
LULC	https://earthexplorer.usgs.gov/	Landsat MSS, TM, ETM+, OLI/TIRS	30m	16 days
Carbon pool	http://data.naturalcapitalproject.org/nightly-build/invest-users-guide/html/carbonstorage.html,Literature	Aboveground and belowground carbon, soil carbon, carbon density in dead organic matter	–	–
Root depth	http://www.fao.org/soils-portal/soil-survey/soil-maps-and-databases/harmonized-world-soil-database-v12/en/	Root restricting layer depth	30 arc-second	–
PAWC	http://www.fao.org/soils-portal/soil-survey/soil-maps-and-databases/harmonized-world-soil-database-v12/en/	Plant Available Water Content	30 arc-second	–
Watershed	http://www.india-wris.nrsc.gov.in/wrpinfo/index.php?title=WRIS_Publications	Digital watershed atlas of India	–	–
DEM	http://srtm.csi.cgiar.org/srtmdata/	Elevation data	–	–
Soil data	http://www.fao.org/soils-portal/soil-survey/soil-maps-and-databases/harmonized-world-soil-database-v12/en/	Soil properties including texture and organic matter	30 arc-second	–
Road, rail line	https://www.openstreetmap.org/#map=5/47.428/22.676	Road, railway line, state and national highway, location of urban centre, residential centre	–	–
Biophysical tables	http://releases.naturalcapitalproject.org/invest-userguide	For InVEST carbon sequestration, water yield, sediment delivery, habitat quality, and nutrient delivery models	–	–

open street map (https://www.openstreetmap.org/#map=5/47.428/22.676). Demographic information of the study region including population and population density was derived from district statistical handbook (https://www.wbpspm.gov.in/publications/District%20Statistical%20Handbook).

To evaluate the performance of NPP models, one-sample and paired sample Student's t parametric tests were performed. A total of ten pairs of the model were prepared to measure the similarity of model estimates. Additionally, several statistical techniques including the coefficient of determination (R^2), root mean square of error (RMSE), mean absolute percentage error (MAPE), Durbin Watson (DW), Mallows Cp coefficient, Akaike information criterion (AIC), and Schwarz's Bayesian information criterion (SBC) were utilized to evaluate the trade-offs and synergies among the ESs.

2.3. Estimation of net primary production using light use efficiency models

In this study, five ecosystem production models were adopted, including Carnegie Ames Stanford Approach (CASA), Eddy Covariance Light Use Efficiency Model (ECLUE), Vegetation Photosynthesis Model (VPM), Moderate Resolution Imaging Spectroradiometer Model (MOD17), and Global Production and Efficiency Model (GLO-PEM), to estimate net primary production (NPP) and ESs. The description of the datasets is provided in Table 1.

2.3.1. CASA model

The Carnegie-Ames-Stanford-Approach (CASA) model developed by Potter et al. (1993) has been widely used in the literature to estimate NPP (gC m^{-2} $year^{-1}$) using remotely sensed satellite data, meteorological inputs (temperature, precipitation, solar radiation), surface and atmospheric moisture stress factors (land-water stress, vapor pressure deficit, land surface temperature) (Crabtree et al., 2009; DeFries et al., 1999; Ruimy et al., 1999; Cramer et al., 1999; Seixas et al., 2009). In this model, NPP is the function of Absorbed Photosynthetically Active Radiation (APAR MJ m^{-2} $year^{-1}$) and light use efficiency (LUE gC MJ^{-1}). APAR is the function of photosynthetically active radiation (PAR MJ m^{-2} $year^{-1}$) and a fraction of APAR, the latter of which is derived from the linear approximation of normalized difference vegetation index – NDVI and alternatively from enhanced vegetation index – EVI. PAR is the half of incoming shortwave solar radiation (MJ m^{-2} $year^{-1}$). Additionally, the actual LUE is affected by the water stress factors derived from the ratio of actual and potential evapotranspiration, and the temperature stress factor derived from the deviation of maximum, minimum, and optimum temperatures from the ideal condition. Details about the model parameterization, input data are given in Tables S1 and S2.

2.3.2. EC-LUE model

The Eddy Covariance-Light Use Efficiency model, developed by Yuan et al. (2007), assumes that vegetation productivity controlled by the limiting factors (surface moisture and air temperature) at any given time. This model has been successfully applied in various eco-regions across the world (Yuan et al., 2007, 2014; Xie et al., 2019; Zhang et al., 2015) to estimate spatiotemporal Gross Primary Productivity (GPP) and other carbon estimates. In this model, GPP (gC m^{-2} $year^{-1}$) is the function of fPAR, PAR, and Liebig minimum temperature stress derived from the ration of average, minimum, maximum, and optimum temperatures, and water stress derived from the ratio of latent heat and sensible heat.

2.3.3. VPM model

The vegetation photosynthesis model (VPM) developed by Xiao et al. (2004) assumes that LUE of plant canopy depends on the

temperature sensitivity, moisture sensitivity, and leafage of a canopy. The water stress factor used in this model is derived from the ratio of actual and maximum land surface water index (LSWI).

2.3.4. GLO-PEM model

The Global Production Efficiency Model (GLO-PEM) developed by Prince and Goward (1995) has been successfully used in several ecosystems across the world to estimate terrestrial NPP and GPP (Wang et al., 2014; Zhang et al., 2015). In this model, GPP is the function of fPAR, PAR, temperature stress factor (same as VPM model), water stress factor (same as ECLUE model), and vapor pressure deficit (VPD), which can be calculated from actual and saturated vapor pressure estimates.

2.3.5. MOD17 model

The MOD17 GPP model (Running et al., 2004, 2014) is based on the function of fPAR, PAR, maximum LUE, land cover, vapor pressure deficit (VPD) and the temperature stress factor (Running et al., 2004). The biome-specific LUE for each ecosystem was approximated according to the results of Yuan et al. (2014) and Running et al. (2004, 2014). The detail descriptions about the ecosystem models are given in Sannigrahi et al. (2018).

2.4. Classification and prediction of LULC with machine learning algorithms

2.4.1. Classification of LULC for past and current years

To obtain the best land classification estimates for valuation and quantification of multiple ESs, 10 machine learning algorithms were used for classifying the regions into several identical ecosystem units that match the existing global and regional land cover classification schemes. These models include Artificial Neural Network (ANN), Bayes, Decision Tree (DT), Gradient Boosted Tree (GBT), Linear Discriminant Analysis (LDA), K Means Nearest Neighbour (KNN), Maximum Likelihood Classifier (MLC), Random Forest (RF), Support Vector Machine (SVM) Linear, and Radial Basis Function (RBF). The classification for five reference years, including 1973, 1988, 2003, 2013, and 2018 was performed. The details of classification methods, accuracy assessment, and model evaluation are discussed in Sannigrahi et al. (2019a).

2.4.2. Prediction of future LULC

Using the existing land use information, future land use scenarios were predicted using the Cellular Automata Markov Chain (CA-Markov) model. Landsat Multi-Spectral Scanner (MSS), Landsat 5 Thematic Mapper (TM), Landsat 7 Enhanced Thematic Mapper (RTM), and Landsat 8 Operational Land Imager (OLI) and Thermal Infrared Sensor (TIRS) Tier 1 geometrically and radiometrically processed data (except Landsat MSS) were used for image classification and subsequent analysis. Both area-based and pixel-based accuracy assessment approaches were applied for evaluating the accuracy of classification estimates and model performances (Sannigrahi et al., 2019b). Several similarities and dissimilarity matrices were used for assessing the inter-model consistency and strength-weakness of the algorithms. High-resolution Google Earth images were used for the thematic accuracy assessment and model evaluation. Post classification approaches, such as majority filter, boundary clean, nibble, and set null, were applied for removing isolated pixels from classification estimates. The details about the machine learning models used for LULC classification, accuracy assessment, and (dis)similarity assessments have been provided in Sannigrahi et al. (2019a).

For the future prediction of LULC and ESVs, the CA-Markov model and Integrated Valuation of Ecosystem Services and Trade-off (InVEST) were used in this study. The LULC maps of 2003 and 2013 were used to compute the transition probability matrix using the Markovian transition estimator module and to produce the projected LULC map for 2018. A total of 10 driving variables, including distance to rail line, distance to road, distance to highway, distance to urban center, distance to residential center, distance to water surface, distance to urban activity center, DEM, slope, population density, were utilized to produce the transition suitability maps (Hou et al., 2019). After combining the Markovian transition suitability matrix and CA-based transition suitability maps, the area of different LULC categories for multiple reference years was then estimated. After that, the accuracy of the projected LULC with the existing LULC derived from the machine learning model was evaluated. The CA-Markov model calculated potential area transitional probabilities for different land classes, which are discussed in Table S5. The other reference information including sample features for each identical land use class retrieved from Google Earth imagery, existing land use maps of the study region, was also utilized for analyzing the accuracy of the projected LULC map. After deriving satisfactory estimates between the reference and classified maps, the Markov transition matrix was applied in the next step to simulate the future land cover maps, ESs, and ESVs for 2025, 2035, and 2045.

2.5. Estimations of biophysical and economic values of multiple ESs

2.5.1. Gas regulation service

The gas regulation services of a natural capital can be measured with three methods: (1) photosynthesis and respiration formulae; (2) test and survey method; (3) a mathematical model (Guo et al., 2001). In this study, the standard photosynthesis and respiration equation was used to estimate the economic values of gas regulation services as follows:

$$\begin{aligned} &CO_2(264g) + H_2O\,(108g) \\ &\rightarrow C_6H_{12}O_6\,(180g) + O\,(193g) \\ &\rightarrow Amylase\,(162g) \end{aligned} \quad (1)$$

Where CO_2 and H_2O are the carbon-di-oxide and water components, respectively; C, H and O are Carbon, Hydrogen, and Oxygen components, respectively.

The amount of Oxygen released by a green canopy to produce 1g of dry matter is approximated as 1.2g. Using these the two components, i.e., carbon capture and oxygen release, the gas regulation service was estimated as follows:

$$GR_v = (1.62 * NPP * PCO_2) + (1.2 \times NPP \times PO_2) \quad (2)$$

Where GR_v is the economic value (US $) of gas regulation services; NPP is the net primary productivity (gC m^{-2} $year^{-1}$) of a pixel; PCO_2 and PO_2 are prices of carbon sequestration (the social cost of carbon value, which is 315.62US$ ton C for India, was used in this study as a proxy) and oxygen production (125 US$ ton O_2 in India); the values of 1.62 and 1.2 are the equivalent values derived from photosynthesis equation (Song et al., 2015a; Xiao et al., 2005; Ricke et al., 2018; Sun et al., 2016).

2.5.2. Climate regulation service

Two different methods were employed to estimate the biophysical and economic values of climate regulation service. The first method is based on the calculation of NPP. The spatiotemporal NPP was estimated using five ecosystem models. Later on, the biophysical values of NPP (ton C) was used as a proxy to estimate the climate regulation service as follows:

$$NPP_{(x,t)} \times \ C_p \tag{3}$$

Where *NPP* is the net primary productivity value (ton); x, t are the particular pixels and time; C_p is the price of carbon. In this study, the social cost of carbon value (315.62 US$ ton C) was used as a proxy of the carbon price (Ricke et al., 2018). The information on carbon pools was derived from published literature and model user's documentation (Tables S6 and S6).

2.5.3. Disturbance regulation service

The flood disturbance is associated with the capacity of the landscape to regulate the excess water that enters the landscape due to floods (Carreño et al., 2012). This also depends on the occupancy of the water surface, which can expand and absorb the impact of water excess. There are several proxies being used to compute the economic values of disturbance or water regulation services. Among them, the cost of reservoir/dam construction value was used in this study. Two components, the occupancy of water bodies in the landscape and water input into the system (precipitation), were utilized to compute the disturbance regulation service, formulated as follows:

$$DR_v = I_w + \ O_w \ + \ 1.25 + \ P_{DC} \tag{4}$$

Where DR_v is the value disturbance regulation; I_w is the water input into the system (precipitation); O_w is the water bodies occupancy percentage; the value of 1.25 is the correction factor; $P_{DC}$is the price of dam construction (0.24 US$ m^{-3}) (http://cwc.gov.in/national-register-large-dams).

2.5.4. Water regulation and water yield service

The distribution of different LULC types can have a significant impact on surface water flow. Most of the agrometeorological variables including actual and potential evapotranspiration, water use efficiency, water retention efficiency, and runoff potential are directly or indirectly determined by the land-use variation (Blumstein and Thompson, 2015). Therefore, a proper assessment of the changes in land-use patterns and their effects on surface water flow is highly needed (Krause et al., 2008). The hydrological regulation and water purification are two main components that need to be measured separately to quantify the per unit water conservation (WC) service of a region. The hydrological regulation denotes the retention of surface water flows by a green substance in ecosystems. In this study, the economic values of water conservation service using the equation of surface water balance was calculated as follows:

$$WR_v = \ 10C_iA_i \ (P_i - \ E_i - \ C_i) \tag{5}$$

Where WR_v is the value of water conservation service; $C_i$is the cost of reservoir construction (0.24 US$ m^{-3} in India) (http://cwc.gov.in/national-register-large-dams); $A_i$is the area of ecosystem type; $P_i$is the precipitation (mm $year^{-1}$); $E_i$is the evapotranspiration (mm $year^{-1}$); $C_i$is the surface runoff (mm $year^{-1}$) (Hu et al., 2018; Xu et al., 2018; Yang et al., 2018). Here, the surface runoff C_i can be determined by rainfall, a number of rain events, land use land cover types, and soil types (Xu et al., 2018).

Additionally, in this study, the InVEST 3.4.4 Water Yield Model was incorporated to estimate the biophysical values of water yield service of the Sundarbans region. Several studies revealed that the InVEST water yield model has a high level of accuracy when predicting the surface water flow at the landscape scale (Redhead et al., 2016; Hu et al., 2018). According to the surface water balance principle, the water yield of an ecosystem is equivalent to the difference between precipitation and actual evapotranspiration. This model also includes the effects of other variables, i.e., availability of soil moisture, surface water flow, water retention capacity of green canopy, and canopy interception on water yield capacity and associated water conservation service. The other input variables of the InVEST water yield model include root depth, plant available water content (PAWC), land use and land cover, watershed, and sub-watershed, which are given in Table 1. The model default value 7 was selected as the Z parameter (Hu et al., 2018). In InVEST water yield model, the actual evapotranspiration was calculated using the approach proposed by Zhang et al. (2001) and Budyko's hypothesis, shown as follows:

$$Y_{xj} = \left(1 - \frac{AET_{xj}}{P_x}\right) \times P_x \tag{6}$$

Y_{xj} is the water yield of land use type j and pixel x; $AET_{xj}$is the actual evapotranspiration (mm) of land use type j and pixel x; $P_x$is the precipitation (mm) of pixel x. The AET_{xj}/P_x was approximated using the Budyko's curve principle, shown as follows:

$$\frac{AET_{xj}}{P_x} = \ \left(\frac{1 + \ \omega_x R_{xj}}{1 + \ \omega_x R_{xj} + (1/R_{xj})}\right) \tag{7}$$

Where $R_{xj}$are the Budyko index of dryness for land use type j and pixel x, and the Budyko dryness is based on the ratio between potential evapotranspiration (mm) and precipitation (mm); $\omega_x$is the dimensionless ratio of plant available water content to accumulated annual rainfall, which can be estimated as follows:

$$\omega_x = \ Z\frac{AWC_x}{P_x} \tag{8}$$

Where AWC_x is the volumetric plant available water content (mm); *Z*is the seasonality factor which captures the precipitation and other hydrological patterns and characteristics. Additionally, Budyko's dryness index can be calculated as follows:

$$R_{xj} = \ \frac{k_{xj}ETo_x}{P_x} \tag{9}$$

Where $k_{xj}$is the evaporation factor for land use type j and pixel x; $ETo_x$is the reference evapotranspiration of pixel x (Carreño et al., 2012; Yu and Han, 2016; Hu et al., 2018; Xu et al., 2018; Lang et al., 2017). The ETo_x is derived from the Hargreaves-Samani 4 method as follows:

$$ETo_x = 0.0009384R_a \times (T_{max} - T_{min})^{0.424} \times (T + 17.8) \tag{10}$$

Where $R_a$is the incoming shortwave solar radiation (MJ M^{-2}); T_{max}, T_{min}, and T are the maximum, minimum, and average temperatures (°C), respectively (Valipour, 2015; Trajkovic, 2007).

2.5.5. Soil conservation service

The InVEST SDM model uses a comprehensive approach to estimate the per pixel soil erosion, soil retention by the downstream surface vegetation, and sediment export, respectively. The SDM first calculates the quantity of annual soil loss of a pixel, then quantify the resultant sediment delivery ratio (SDR), which is the proportion of soil that gets eroded and eventually reached to the downstream. After settling the eroded sediments into the stream, it would finally end up at the downstream catchment outlet (Sharp et al., 2018; Tallis et al., 2011). To calculate the amount of soil conserved, the annual actual and potential soil loss was estimated for 1973, 1988, 2003, 2013, 2018, 2025, 2035, and 2045 reference

years using Revised Universal Soil Loss Equation (RUSLE) and SDM. The specific inputs required to run the SDM include digital elevation model (DEM), rainfall erosivity index derived from precipitation, soil erodibility derived the soil type data, land use land cover types for estimating the management factor. The SDM and RUSLE can be mathematically described as:

$$A = R_i * K_i * LS_i * C_i * P_i \quad (11)$$

Where $A$is the actual annual soil loss (tons ha^{-1} year^{-1}); $R_i$is the rainfall erosivity factor (MJ mm ha^{-1} h^{-1} year^{-1}); $K_i$is the soil erodibility factor (ton ha h MJ^{-1} mm^{-1} ha^{-1}); $LS_i$is the slope and steepness factor (unitless); $C_i$is the crop management factor (unitless); $P_i$is the support practice factor (unitless). After that, the potential annual soil loss was estimated as follows:

$$\Delta A = R_i * K_i * LS_i \quad (12)$$

Where $\Delta A$is the potential annual soil loss (tons ha^{-1} year^{-1}). Followed by, the amount of soil retention was estimated as follows:

$$SR_i = \Delta A - A \quad (13)$$

Where $SR_i$is the amount of annual soil retention (tons ha^{-1} year^{-1}). The soil erodibility factor was estimated as follows:

$$K = 0.1317 \times \left\{0.2 + 0.3\ \exp\left[\frac{-0.0256SAN(1-SIL)}{100}\right]\right\} \times \left(\frac{SIL}{CLA+SIL}\right)^{0.3} \times \left[1.0 - \frac{0.25C}{C + \exp(3.72 - 2.95C)}\right] \times \left[1.0 - \frac{0.7SNI}{SN1 + \exp(-5.51 + 22.9SNI)}\right] \quad (14)$$

Where SAN, SIL, and $CLA$are the sand, silt, and clay fraction (%); $C$is the soil organic carbon content (%); $SNI$is equal to 1− SAN/ 100 (Jiang et al., 2016; Fang et al., 2018; Zhang et al., 2017). The steepness and slope (LS) factor can be estimated as follows:

$$S = \left(\frac{\sin\theta}{0.0896}\right)^{0.6}$$

$$L = \left(\frac{\lambda}{22.13}\right)^{m}$$

$$\begin{aligned} m &= 0.05 && \theta \geq 9 \\ m &= 0.04 && 9 > \theta \geq 3 \\ m &= 0.03 && 3 > \theta \geq 1 \\ m &= 0.02 && 1 > \theta \end{aligned} \quad (15)$$

Where $\lambda$is the slope length (m); $m$is the slope length coefficient; θ is the gradient (Su et al., 2012; Fang et al., 2018). Followed by, the annual rainfall erosivity factor was estimated as follows:

$$\begin{aligned} R &= 0.0483P^{1.610} && P < 850mm \\ R &= 587.8 - 1.219P + 0.004105P^2 && P \geq 850mm \end{aligned} \quad (16)$$

Where $P$is the annual rainfall (mm) (Renard and Freimund, 1994; Lee and Heo, 2011). The cover management and support practice factors were approximated using the approach presented by Cerretelli et al. (2018). The threshold flow accumulation, Borselli k parameter, Borselli IC0 parameter, and max sediment retention (SDR) value were chosen as 1000, 2, 0.5, and 0.8. Additionally, the per-pixel sediment delivery ratio (SDR) and sediment export were estimated as follows:

$$SDR_i = \frac{SDR_{max}}{1 + \exp\left(\frac{IC_0 - IC_i}{k}\right)} \quad (17)$$

$$\begin{aligned} SE_i &= RUSLE_i \times SDR_i \\ SE &= \sum_i SE_i \end{aligned} \quad (18)$$

Where $SDR_i$is the sediment delivery ratio of the pixel i; $SDR_{max}$is the maximum SDR, and $k$are the calibration parameters; $IC_i$is the connectivity index of pixel i; $SE_i$is the sediment export (ton ha^{-1} year^{-1}) from pixel i; $SE$is the total catchment sediment export (ton ha^{-1} year^{-1}).

For estimating the economic value of soil conservation service, the valuation of soil fertility and productivity approach was adopted in this study. The information about the three principal soil fertilizer components including the Nitrogen (N), Phosphorous (P), and Potassium (K) was aggregated, and subsequently, the value of soil conservation was estimated as follows:

$$V_{SC} = \sum_{i-1}^{n} SR_i \times C_i \times P_i \quad (19)$$

Where $V_{SC}$is the economic value of soil conservation service; $SR_i$is the annual soil retention of pixel i; $C_i$is the N, P, K content in the soil, which is N = 0.0478%, P = 0.0563%, and K = 1.8%,$P_i$is the price of N, P, and K (Kibria et al., 2017a; Song et al., 2015b; Carreño et al., 2012). The no-data pixels for all the raster layers used as inputs in the InVEST SDR model were assigned as 0. Additionally, the LULC layer was converted to integer format, and other inputs were converted to floating format to conduct the SDR model. The row, column, and cell size of the given inputs were kept the same for all the images used in this model.

2.5.6. Nutrient control service

The Nutrient Delivery Ratio (NDR) model depicts the land use and climatic change effects on the surface nutrient loss and resulting water quality of an ecosystem (Tallis et al., 2011). For estimating the per pixel nutrient retention (NR), the InVEST 3.4.4 NDR model was used. The NDR model needs raster and vector inputs including digital elevation model (DEM), land use and land cover (LULC) types, nutrient runoff proxy (precipitation), watershed and sub-watershed layers, a biophysical table that includes the load of nutrient, the nutrient retention efficiency, and critical length information for each ecosystem. The NDR model estimated the per unit NR using four steps: (1) the average annual water yield was estimated for each ecosystem types; (2) the average yearly

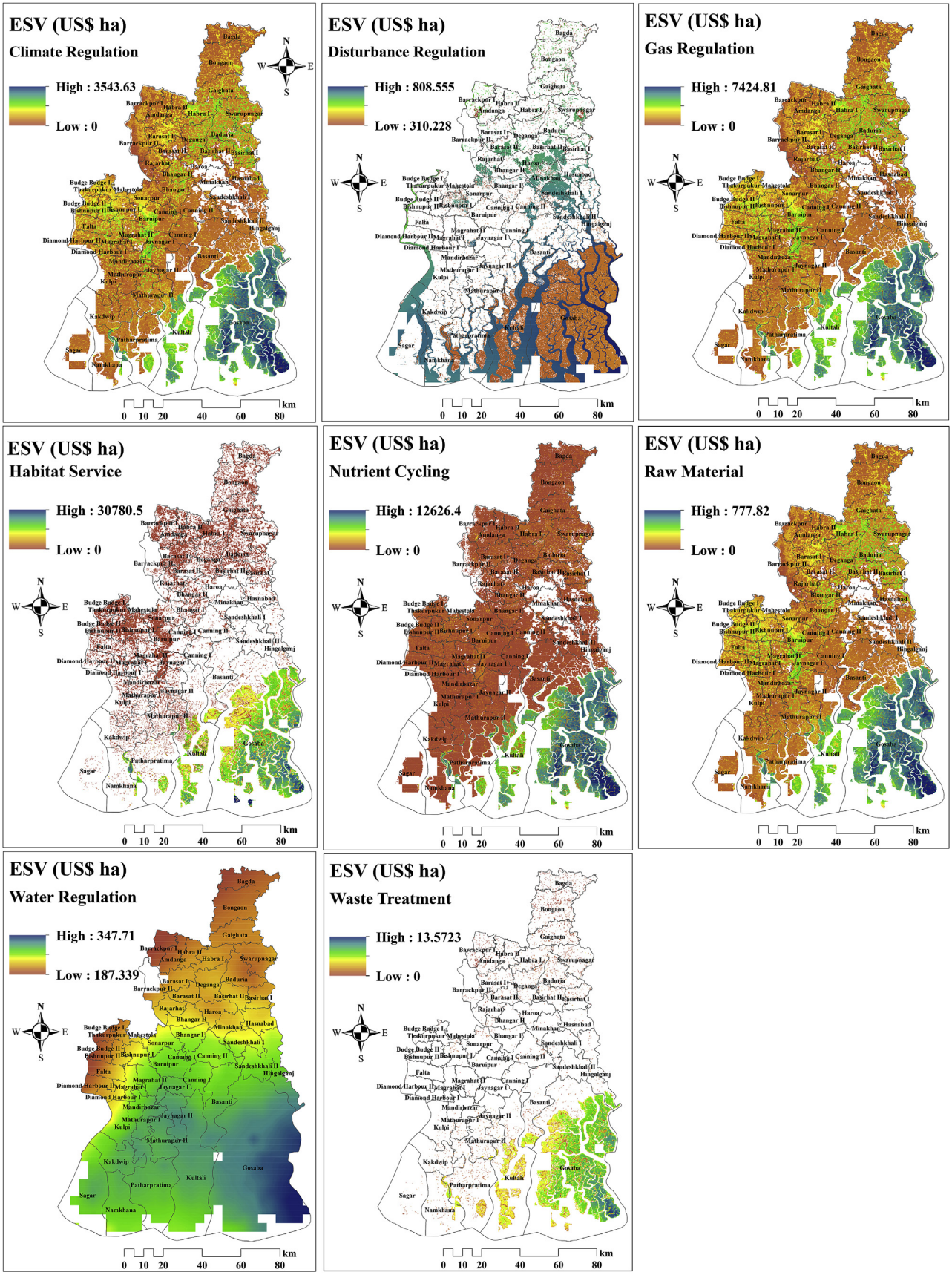

Fig. 2. Spatial distribution of the ecosystem service values of different ecosystem services.

nutrients that exported from each ecosystem types were calculated using the equivalent value derived from literature; (3) the nutrient load is estimated using the routing water along the path; finally, (4) the amount of nutrients retained by the green vegetation was estimated using the nutrient retaining efficiency values approximated for each LULC (Yang et al., 2018; Rukundo et al., 2018; Cabral et al., 2016). The information about the threshold accumulation value, Borselli k parameter, subsurface critical length for N and P, subsurface maximum retention efficiency for N and P is given in Table S8.

The economic value of the nutrient cycling service is derived from the NPP based estimates as follows:

$$NC_V = \sum NPP_x \times R_{i1} \times R_{i2} \times P_i \quad (20)$$

Where NC_V is the economic value of nutrient cycling service; NPP_x is the net primary productivity (ton ha^{-1}) value of pixel x; R_{i1} is the distribution rate of the major nutrient elements N, P, K in organic matter for different LULC; R_{i2} is the converted coefficients of N, P, K to corresponding chemical fertilizer; P_i is the price of N, P, K. The values of $R_{i2}N$, $R_{i2}P$, and $R_{i2}K$ were approximated as 2.14, 6.55, and 1.91, respectively (Kibria et al., 2017). The $R_{i1}N$, $R_{i1}P$, $R_{i1}K$ were derived based on the methods by (Ray, 2018; Ray et al., 2014, 2015) (http://www.iiss.nic.in/mapd_7.htm).

2.5.7. Waste treatment service

The economic values of waste treatment service of the natural capitals were separately calculated in this study, as derived from the function of annual NPP (ton ha), annual precipitation, and water bodies occupancy percentage as follows:

$$WT_V = NPP \times (1 - CV_{NPP}) \times I_w \times O_w \times 1.75 \times P_{wt} \quad (21)$$

Where WT_V is the economic value (US$ ha^{-1}) of waste treatment service; NPP is the net primary productivity (ton ha^{-1}); CV_{NPP} is the coefficient of variation of NPP; I_w is the water input into system (0–1); O_w is the water bodies occupancy percentage; P_{wt} is the average waste treatment cost (Wang et al., 2010; Carreño et al., 2012; Yu and Han, 2016; Zhang et al., 2017; Watson et al., 2016).

2.5.8. Raw material provision service

The biophysical values of raw material provision service were derived from the NPP estimates. The NPP is a proxy for evaluating the global and local climate regulation as it depicts the net carbon uptake from atmosphere and oxygen releases into the atmosphere. In this study, the richness of biomass and the provision of organic materials were quantified from the annual NPP estimated for different ecosystem types. Multiple ecosystem production models were implemented to estimate the spatiotemporal NPP. Additionally, the economic value of raw material production service was calculated using the energy substitution approach proposed by Song et al. (2015a), shown as follows:

$$V_{RM} = NPP_i \times P_{RM} \quad (22)$$

Where V_{RM} is the economic value of raw material provision service; NPP_i is the net primary productivity of pixel i; P_{RM} is the price of raw material calculated as follows:

$$P_{RM} = NPP_i \times 2.2 \times 0.67 \times P_{SC} \quad (23)$$

Where P_{SC} is the price of standard coal ($\approx$3000 INR in 2015) (Coal India Limited, Govt. Of India, 2015). The production of raw material is derived from the NPP using the following approximation: 1 g of carbon = 2.2 g of organic matter (Song et al., 2015a). Subsequently, using the energy substitute approach, the amount of energy available in one unit of organic biomass is derived from the following approximation: 1 g organic matter is equal to 0.67 g of standard coal (Song et al., 2015a).

2.5.9. Biological control/biodiversity management

Using the landscape scoring approach (Burkhard et al., 2009, 2014) and NPP based proxy method, the biophysical and economic values of biological control (BC) and biodiversity management (BDM) services were estimated. A total of eight experts were chosen based on their familiarity and awareness of the research problem. The calculation of the services is given below:

$$BC = A_k \times \sum_{i=1}^{n} BC_j \times \sum_{i=1}^{n} VC_{jk} \quad (24)$$

$$BDM = NPP \times (1 - CV_{NPP}) \times I_w \times W_f \times 1.75 \quad (25)$$

Where BC is the biological control service; A_k is the area of land use type k; BC_j is the capacity of different landscapes to provide ecosystem service j (expert score for wildlife abundance was selected for estimating BC service); VC_{jk} is the adjusted value coefficient for land use type k and ecosystem service j, derived from Sannigrahi et al. (2019a); BDM is the biodiversity management service; CV_{NPP} is the coefficient of variation of NPP; I_w is the water input into the system (precipitation, value ranges from 0 to 1); N_f is the naturalness factor; the value of 1.75 is the multiplicative factor (Barral and Oscar, 2012; Carreño et al., 2012; Zhang et al., 2017).

2.5.10. Habitat provision

To quantify the biophysical and economic values of habitat provision service, the InVEST 3.4.4 habitat quality model and biomass-based proxy approaches were used. NPP was used as a proxy to quantify the per unit biomass of the study region. The annual rainfall and temperature data were used for evaluating the effects of climatic factors on habitat provision. The final calculation is described below:

$$HP = NPP_i \times (1 - CV_{NPP}) \times F_{PRE} \times F_{TEMP} \times (1 - F_{ALT}) \quad (26)$$

$$V_{HP} = HP \times P_{HP} \quad (27)$$

Where HP is the biophysical value of habitat service; CV_{NPP} is the coefficient of variation of NPP; F_{PRE} is the favorable precipitation; F_{TEMP} is the favorable temperature; F_{ALT} is the altitude, V_{HP} is the economic value of habitat service; P_{HP} is the price of habitat service (derived from Sannigrahi et al., 2019b). Additionally, the InVEST habitat suitability model was also used to quantify the biophysical values of habitat provision service, and the details are given in Tables S9 and S10.

2.5.11. Cultural service

The cultural ecosystem services (CES), including aesthetic, tourism, recreation, educational, spiritual, inspiration and social relations, are often conceived as the nonmaterial opportunities and benefits brought by natural capitals that are as important as its counterparts including the regulating, supporting, and provisional services (MA, 2005). Using the landscape capacity scoring approach proposed by Burkhard et al. (2009, 2014), the economic value of CES was estimated as follows:

Fig. 3. The biophysical values of different ecosystem services derived from InVEST model.

Table 2
Total carbon storage estimates (Mg C) for different reference years.

Year	Total Carbon storage (Mg C)			Net Present value from current to future (US$)
	Current	Future	Changes	
1973	78331769.38	78521069.19	461692.21	94673480.19
1988	78521069.19	79633984.38	1104463.01	226478635.8
2003	79633984.38	77009844.88	−2624137.83	−622434537.1
2013	77009844.88	81692843.15	4697569.7	1300937089
2018	81684981.32	82493356.19	808367.19	210179528
2025	82493356.19	83647453.32	1154099.75	273747568.2
2035	83647453.32	84678479.19	1031024.82	244554686.6
2045	84678479.19	–	–	–

$$V_{CES} = A_k \times \sum_{i=1}^{n} CES_j \times \sum_{i=1}^{n} VC_{jk} \quad (28)$$

Where $V_{CES}$is the value of cultural ecosystem service; $A_k$is the area (ha) of land use type k; $CES_j$is the capacity of different landscapes to provide ecosystem services *j*; $VC_{jk}$is the adjusted values coefficient of ecosystem service type j and land use type k. An expert opinion survey was conducted to estimate the score of each landscape to provide the necessary ecosystem services. Totally eight experts were selected to obtain their responses. Subsequently, a landscape score matrix was prepared where the x (row) axis represents different land-use types, and the y-axis (column) represents the types of ecosystem services. Using the 5 point Likert scale method, (0 = no relevant capacity, 1 = low relevant capacity, 2 = relevant capacity, 3 = medium relevant capacity, 4 = high relevant capacity and 5 = very high relevant capacity), the score for the relevant services were attained. The experts involved in the scoring process were suggested to provide scores for each landscape depending on their capacity to provide multiple ecosystem services. The details of the expert score are given in Table S11. The adjusted value coefficients (VC_{jk}) for different land-use types were retrieved from Sannigrahi et al. (2019a).

2.6. Estimation of (non)spatial trend of biophysical variables and ESs

The spatiotemporal changes of different biophysical variables (e.g., EVI, NDVI, fPAR, NPP), climatic variables (i.e., precipitation and temperature), and ESs during the 1982–2017 (36 years) were analyzed. The seasonal and annual variations of EVI, NDVI, and fPAR were evaluated to understand the climatic effects on ecosystem productivity. Average 23–24 MODIS EVI/NDVI time-series data layers for each year were integrated for estimating the annual variation of EVI/NDVI during 2000–2017. Additionally, to examine the long term seasonal and annual changes of the principal biophysical variables including NDVI, EVI, fPAR, and NPP during 1982–2017 in the Sundarbans region, pixel-level spatiotemporal trends were calculated using the ordinary least squares (OLS) regression approach. The directional (both positive and negative) changes of the aforementioned biophysical components were examined through the estimated slope values for each pixel. The OLS method has deemed a robust and comprehensive approach to evaluate the long-term dynamics of biophysical variables of an ecosystem (Leroux et al., 2016). In this study, the OLS considered time as an independent variable and pixel-level EVI/NDVI/fPAR/NPP as response variables in order to perform the time-lagged and continuous trend analysis, which is represented as follows:

$$y = \alpha + \beta.T_i \quad (29)$$

Where *y*is the time series least square estimates; $\alpha$is the model intercept; $\beta$is the spatiotemporal slope of EVI/NDVI/fPAR/NPP during 1982–2017; $T_i$is the MODIS data collection year (Li, 2012; Leroux et al., 2016; Verbesselt et al., 2010; Fang et al., 2018; Jacquin et al., 2010). Additionally, to analyze the time series trends of the meteorological and biophysical variables, the rank-based non-parametric Mann-Kendall (MK) test was performed. The "Kendall" package for R statistical software was applied to conduct the MK test. Additionally, the spatial (i.e., pixel-level) trend and slope of the response variables were also evaluated using the python ArcPy package.

2.7. Calculation of time-lagged, spatial and non-spatial trade-offs and synergies

To evaluate the spatial and non-spatial synergy and trade-offs among the biophysical variables and ecosystem services, the Pearson correlation test was performed at pixel and grid level for both time series and individual reference years, i.e., 1973, 1988, 2003 and 2017. For the pixel-wise correlation analysis, the ArcPy python package was used. PerformanceAnalytics statistical package for R statistical software was used to measure the Pearson correlation matrix at the grid-scale. Totally 36 data layers (1982–2017, 36 years) were aggregated to perform the Pearson correlation test. Both trade-off (negative correlation) and synergy (positive correlation) associations among the variables were evaluated. For grid-level analysis, the average values of the biophysical variables were extracted at a 3 km*3 km scale using the ArcGIS zonal statistics tool (https://www.esri.com/en-us/home). Followed by, a total of 1481, 1518, 1513, and 1513 sample points were generated for four reference years to evaluate the performance of NPP models. Meanwhile, for pixel-level analysis, a total of 356051, 365898, 377990, and 371356-pixel values were extracted from the corresponding raster layers. These data were assembled for multiple reference years, including 1988, 2003, 2013, and 2017. Additionally, this information was extracted from three ecosystem types, including cropland, mangrove, and mixed vegetation for examining the biome-specific sensitivities of the NPP models.

2.8. Estimation of climate and land use impacts on ESs

The changing climate and degradation of productive land have a significant adverse impact on ESs. However, quantification of such aspects is a challenging task, and the big interest lies in the innovation of new approaches that could estimate the efficient assessment of the disappearance of the valuable ESs that result in monetary loss. Using both InVEST and the CA-Markov model, future losses/gains of land use and ESs were estimated. The biophysical values of five ESs including the carbon sequestration, habitat suitability, water yield, sediment retention, and nutrient retention were estimated for 1973, 1988, 2003, 2013, 2018 as well as for 2025,

Fig. 4. Spatiotemporal changes of the ecosystem services at P < 0.05 level. The black and white colors showing the statistically significant and non-significant changes.

2035, and 2045 reference years. To measure the climate change impact on ESs, current and future predicted precipitation, temperature, and evapotranspiration data were incorporated into the model. The details about the present and future meteorological datasets are given in Table 1. In addition, to evaluate the land-use change effects on ESs, present, and future LULC data were combined with the spatially explicit InVEST model. Besides, to evaluate the effects of the 10 explanatory variables that were used for performing the CA-Markov land-use transition model, the Pearson Correlation coefficient matrix was performed at the P < 0.001 level.

2.9. Univariate local indicators of spatial association (LISA)

The global Moran's I statistic quantifies the spatial

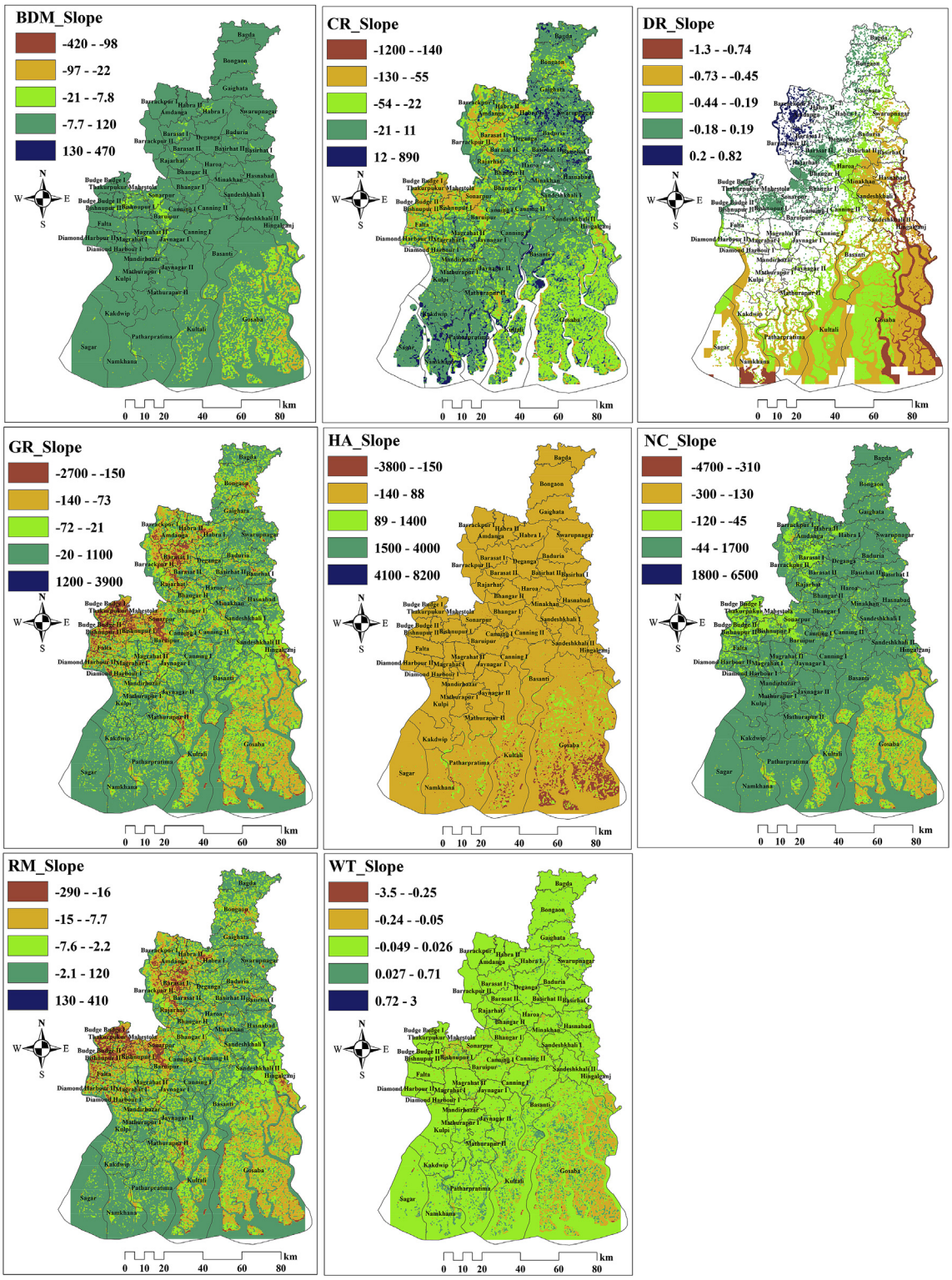

Fig. 5. shows the pixel wise slope of the key ecosystem services. The positive slope indicates the positive changes and negative slope indicates the negative changes of the ecosystem services.

autocorrelation of a distributed features as a whole, while the local indicators of spatial association (LISA) assess the location-specific spatial autocorrelation using local Moran's I index (Anselin, 1995; Levine, 2004; Zhang et al., 2008; Fu et al., 2014). The local Moran's I index has been found to be the most useful indicator to identify the distribution of spatial clusters and spatial outliers (Harries, 2006). The local Moran's I index is narrated as follows:

$$I_i = \frac{z_i - \bar{z}}{\sigma^2} \sum_{j=1, j \neq i}^{n} \left[w_{ij} (z_j - \bar{z}) \right] \tag{30}$$

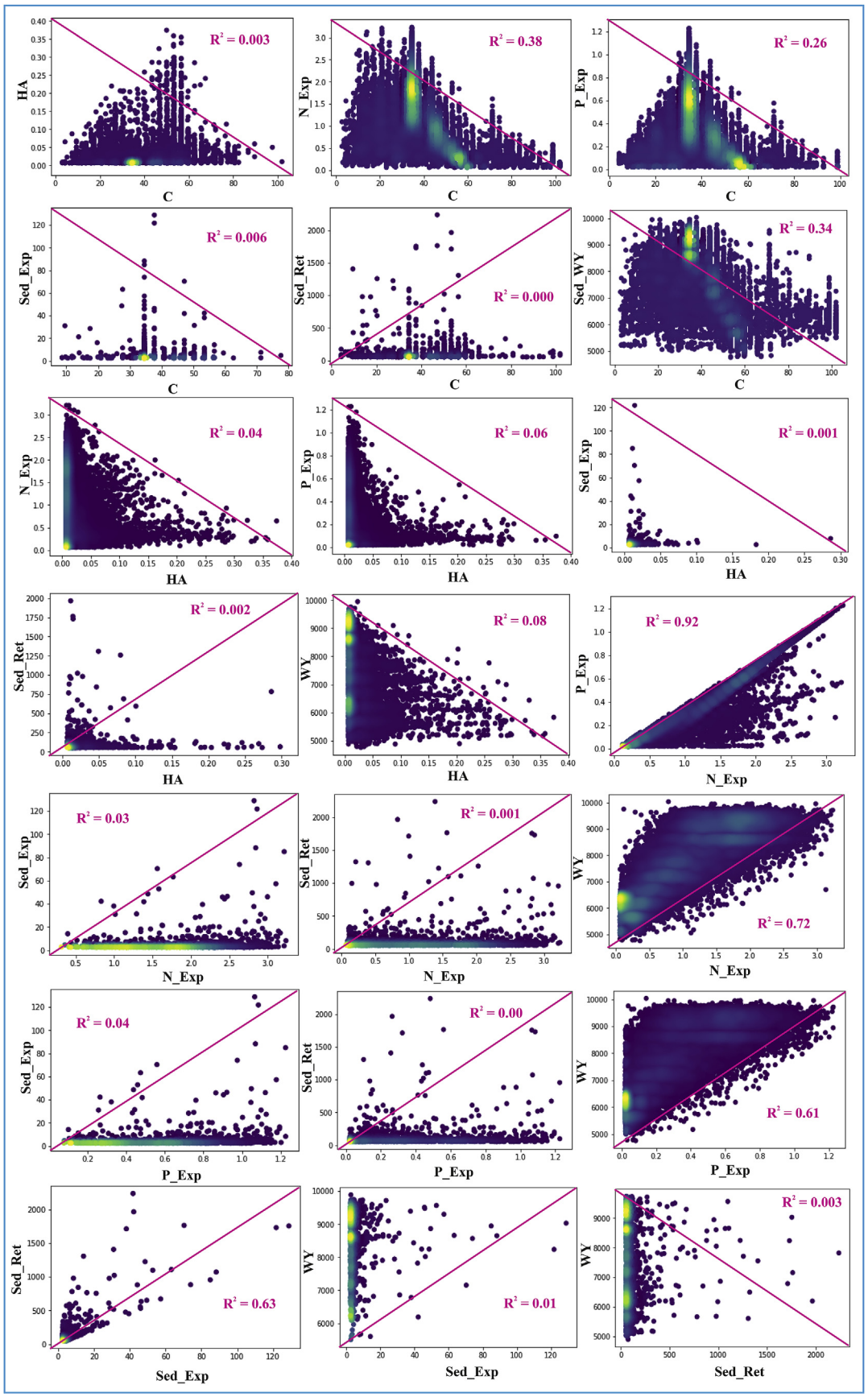

Fig. 6. The 2d scatter density plot showing the linear association between the ecosystem services derived from InVEST model.

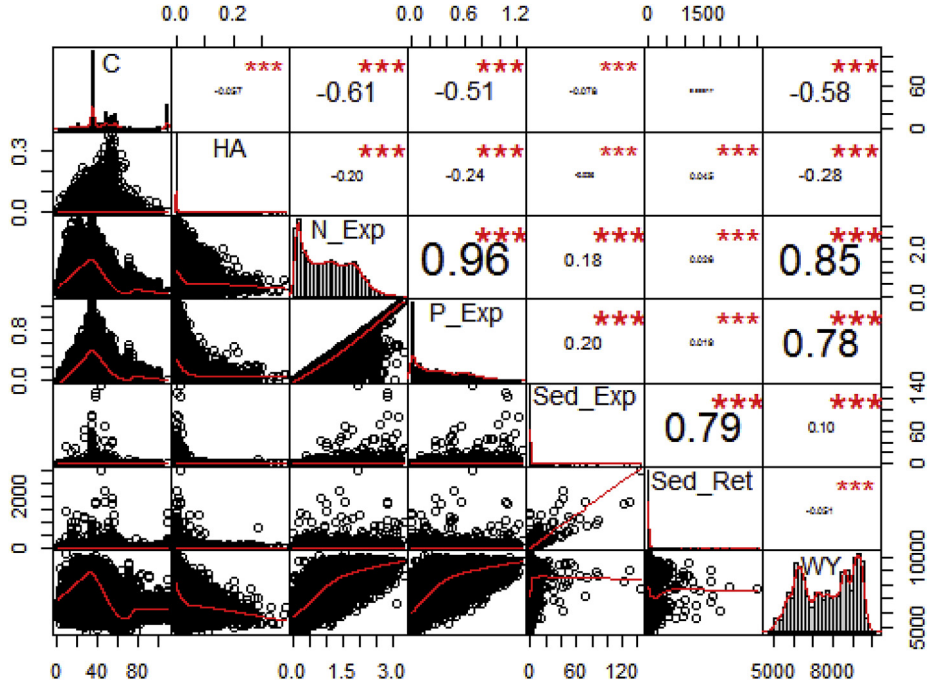

Fig. 7. Pearson correlation matix between the key ESs derived from InVEST model.

$$\sigma^2 = \frac{\sum_{j=1, j\neq i}^{n} (x_j - \overline{X})^2}{n-1} \quad (31)$$

Where $\bar{z}$ is the mean value of z; z_i is the value of the variable at location$i$; z_j is the value at other positions (where $j \neq i$); σ^2 is the variance of z; and w_{ij} is a distance weighting between z_i and z_j, which can be defined as the inverse of the distance. The weight can also be determined using a distance band, namely samples within a distance band are given the same weight, while those outside the distance band are carried the weight of 0; n is the sample number (Zhang et al., 2008; Fu et al., 2014). A high positive local Moran's I value signifies a similar spatial distribution of ESs during the study period (high-high clusters-hotspot and low-low clusters-cold spot) to its neighbours, thus generating spatial clusters of ESs. The occurrence of high−high and low−low clusters can be due to the distribution of high values of ESs with a high value in neighbour states and low values of ESs with a low value in neighbour states, respectively. The spatial outliers of ESs distribution are characterized by a high negative local Moran's I value. This means the spatial distribution of ESs is quite dissimilar from the estimates of their neighbour features. Spatial outliers comprise high−low approximation (island) where a high value of ESs with a low value of ESs in

Table 3
Interaction between major ESs represented by several statistical indicators.

Pair	R^2	RMSE	MAPE	DW	Cp	AIC	SBC	P
C/HA	0.003	0.02	124576.61	1.23	−6006.61	−290137.81	−290129.25	< **0.0001**
C/N_Exp	0.376	1.04	627.27	0.19	−25872.36	2668.76	2677.33	< **0.0001**
C/P_Exp	0.264	0.34	10614.93	0.30	−21891.28	−82360.33	−82351.77	< **0.0001**
C/Sed_Exp	0.006	1.98	348122.37	1.94	−1525.79	52822.90	52831.46	< **0.0001**
C/Sed_Ret	0.000	45.35	558.40	1.96	−2716.79	295157.13	295165.69	< **0.0001**
C/WY	0.338	4282.54	48.62	0.00	−37559.57	647059.18	647067.74	< **0.0001**
HA/N_Exp	0.039	1.23	461.97	0.19	−25872.36	16055.36	16063.93	< **0.0001**
HA/P_Exp	0.056	0.40	2634.67	0.25	−21891.28	−71148.27	−71139.70	< **0.0001**
HA/Sed_Exp	0.001	2.00	224931.58	1.91	−1525.79	53502.77	53511.34	< **0.0001**
HA/Sed_Ret	0.002	46.19	175.82	1.91	−2716.79	296575.62	296584.19	< **0.0001**
HA/WY	0.078	7301.25	89.57	0.15	−37559.57	688340.25	688348.82	< **0.0001**
N_Exp/P_Exp	0.919	0.08	5590.50	0.79	−21891.28	−192761.06	−192752.50	< **0.0001**
N_Exp/Sed_Exp	0.033	1.93	105205.54	2.00	−1525.79	50792.15	50800.72	< **0.0001**
N_Exp/Sed_Ret	0.001	45.42	495.22	1.92	−2716.79	295263.95	295272.52	< **0.0001**
N_Exp/WY	0.715	3563.56	44.17	0.48	−37559.57	632838.16	632846.72	< **0.0001**
P_Exp/Sed_Exp	0.039	1.92	18901.46	2.00	−1525.79	50542.78	50551.34	< **0.0001**
P_Exp/Sed_Ret	0.000	45.62	420.78	1.91	−2716.79	295613.32	295621.88	< **0.0001**
P_Exp/WY	0.610	4349.22	54.22	0.47	−37559.57	648254.68	648263.25	< **0.0001**
Sed_Exp/Sed_Ret	0.627	27.96	55.33	1.81	−2716.79	257741.80	257750.37	< **0.0001**
Sed_Exp/WY	0.011	7598.55	96.81	0.09	−37559.57	691428.62	691437.18	< **0.0001**
Sed_Ret/WY	0.003	7524.79	94.25	0.13	−37559.57	690673.83	690682.40	< **0.0001**

RMSE = Root Mean Square Error; MAPE = Mean Absolute Percentage Error; DW = Durbin Watson; cp = Mallows Cp coefficient; AIC = Akaike's Information Criterion; SBC = Schwarz's Bayesian Criterion.

Table 4
Correlation matrix between the driving factors and biophysical ESs derived from InVEST model.

Variables	C	HA	N_Exp	P_Exp	Sed_Exp	Sed_Ret	WY	PD	UA	RU	ROAD	WB	RES_C	RAIL	HWAY
C	1	−0.032	−0.625	−0.541	−0.086	0.004	−0.595	−0.183	0.469	−0.152	0.604	−0.165	0.165	0.689	0.649
HA	<0.0001	1	−0.210	−0.229	−0.023	0.052	−0.293	0.558	−0.322	−0.215	−0.259	0.014	−0.337	−0.273	−0.262
N_Exp	<0.0001	<0.0001	1	0.969	0.192	0.021	0.847	−0.118	−0.153	0.225	−0.254	0.064	0.095	−0.290	−0.270
P_Exp	<0.0001	<0.0001	<0.0001	1	0.206	0.019	0.786	−0.169	−0.119	0.241	−0.216	0.076	0.123	−0.251	−0.235
Sed_Exp	<0.0001	<0.0001	<0.0001	<0.0001	1	0.772	0.109	−0.021	−0.036	0.046	−0.048	0.009	0.000	−0.054	−0.060
Sed_Ret	0.395	<0.0001	<0.0001	0.000	<0.0001	1	−0.057	0.047	−0.035	−0.016	−0.030	−0.010	−0.042	−0.033	−0.042
WY	<0.0001	<0.0001	<0.0001	<0.0001	<0.0001	<0.0001	1	−0.229	−0.072	0.235	−0.178	−0.008	0.123	−0.175	−0.155
PD	<0.0001	<0.0001	<0.0001	<0.0001	<0.0001	<0.0001	<0.0001	1	−0.503	−0.254	−0.388	0.192	−0.558	−0.478	−0.400
UA	<0.0001	<0.0001	<0.0001	<0.0001	<0.0001	<0.0001	<0.0001	<0.0001	1	0.187	0.811	−0.212	0.551	0.857	0.830
RU	<0.0001	<0.0001	<0.0001	<0.0001	<0.0001	0.003	<0.0001	<0.0001	<0.0001	1	0.153	−0.009	0.209	0.053	0.071
ROAD	<0.0001	<0.0001	<0.0001	<0.0001	<0.0001	<0.0001	<0.0001	<0.0001	<0.0001	<0.0001	1	−0.255	0.465	0.834	0.842
WB	<0.0001	0.006	<0.0001	<0.0001	0.100	0.049	0.108	<0.0001	<0.0001	0.077	<0.0001	1	−0.142	−0.284	−0.315
RES_C	<0.0001	<0.0001	<0.0001	<0.0001	0.960	<0.0001	<0.0001	<0.0001	<0.0001	<0.0001	<0.0001	<0.0001	1	0.360	0.417
RAIL	<0.0001	<0.0001	<0.0001	<0.0001	<0.0001	<0.0001	<0.0001	<0.0001	<0.0001	<0.0001	<0.0001	<0.0001	<0.0001	1	0.895
HWAY	<0.0001	<0.0001	<0.0001	<0.0001	<0.0001	<0.0001	<0.0001	<0.0001	<0.0001	<0.0001	<0.0001	<0.0001	<0.0001	<0.0001	1

C = Carbon storage; HA = Habitat Degradation, N_Exp = Nitrogen Export; P_Exp = Phosphorus Export; Sed_Exp = Sediment Export; Sed_Ret = Sediment Retention; WY = Water Yield; PD = Population Density; UA = Distance to Urban Activity centre; RU = Distance Rural and Urban centre; Road = Distance to Road; WB = Distance to Water Bodies; RES_C = Distance to Residential Centre; RAIL = Distance to Rail line; HWAY = Distance to Highway.

neighbour states, and low–high (atoll) where a low value of ESs with a high value in neighbour states (Zhang et al., 2008; Fu et al., 2014; Palomares et al., 2015; Fan and Myint, 2014). To perform the LISA test, the GeoDa spatial analysis software module was used in this study.

3. Results

3.1. Spatiotemporal distribution and variation of biophysical and climatic variables

The time series trend of NPP and climatic variables (precipitation and temperature) is described in Fig. S1. The average temperature shows an incremental trend from 1982 to 2017, while the annual precipitation has shown a negligible temporal change during the study period. Fig. S2 shows the time-based changes of NPP (gC m^{-2} $year^{-1}$) during the research period. Since there were two different NDVI/EVI data products, one ranges from 1982 to 1999, and the other is extended from 2000 to 2017, the time series trend of NPP for two different periods (1982–1999 and 2000–2017) were evaluated. For the first half, NPP was increased significantly ($R^2 = 0.56$, Adj. $R^2 = 0.53$). The mean NPP (gC m^{-2} $year^{-1}$) was 235 in 1982 which have then increased up to about 286 in 1999. For the second half, a significant decline of NPP was detected ($R^2 = 0.56$, Adj. $R^2 = 0.53$). The average NPP (gC m^{-2} $year^{-1}$) was projected at 346 in 2000, which decreased up to 272 in 2017 (Table S12). Additionally, the time-series changes of NPP derived from the five ecosystem models are found statistically significant at $P < 0.0001$ significance level (Table S3).

The seasonal dynamics of the biophysical variables are shown in Figs. S3 and S4. The peak monthly EVI, NDVI, and fPAR values were observed during the post-monsoon season (September–October – November). The availability of high soil moisture could be the reason for higher NDVI and EVI concentration during this season. However, in 2017, a sharp peak of NDVI is observed during the pre-monsoon period (April–May). This might due to high pre-monsoonal rainfall occurred during this season in 2017. Fig. S5 shows the annual mean NPP (gC m^{-2} $year^{-1}$) derived from five ecosystem models, i.e., CASA, ECLUE, GLO-PEM, MOD7, and, VPM for four reference years. The VPM model has produced the lowest average NPP among the models, followed by MOD17, GLO-PEM, ECLUE, and CASA. Highest NPP was observed in 2003, and a comparatively lower NPP was estimated in 1988 and 2017. A noticeable variation of NPP is evident in this study, and it is due to the uneven distribution of land use and land cover and anomalies of the climatic variables which could be critical determinants of vegetation productivity.

The spatiotemporal changes of the key biophysical (EVI, NDVI) and climatic variables (precipitation, temperature) were assessed through pixel-level trend analysis (Fig. S6). The EVI and NDVI was decline significantly in the western part of Sundarbans and Kolkata suburban region during 1982–2017. Several factors including the urbanization especially over the Kolkata and the surrounding region, mangrove degradation due to severe coastal erosion, increasing salinity especially the western part of the region, could be associated with the declining status of EVI and NDVI observed in this study. In Indian Sundarbans, there are no such ecological restoration policies that could explain the regional vegetation changes and land degradation. However, in the last few decades, a sharp increase of the shrimp aquaculture area is evident in and around Sundarbans which is also detected through time series satellite imageries. This could be the main reason for the declination of EVI/NDVI (regional vegetation change). Since people living in this fragile ecosystem has very limited livelihood options, they are likely to be depended more on the services with direct or marketable benefits, rather than the indirect services provided by mangroves. The changes in precipitation and temperature during 1982–2017 were found statistically not significant (Fig. S6). The paired sample student's t-test also demonstrated that all the ecosystem models employed in this study are statistically different from one another (Table S4). Different model parametrization and conceptual and structural differences among the models could be a reason for these differences.

3.2. Evaluating the performances of ecosystem models

The performance of the five ecosystem models, i.e., CASA, ECLUE, GLO-PEM, MODIS, and VPM was assessed through the Pearson correlation coefficient matrix for four reference years (Fig. S7) and three major ecosystems (Fig. S8). For all reference years, the VPM model has produced a very high association for MODIS and ECLUE model. The MODIS NPP is highly correlated with the GLOP-PEM, and ECLUE derived NPP. Considering the correlation values of five ecosystem models, a weak to the moderate association was observed between VPM NPP/CASA NPP and VPM NPP/GLO-PEM NPP, while the strong association is accounted between the VPM/ECLUE NPP and VPM/GLO-PEM NPP. It was observed that all those models were performed most accurately over the

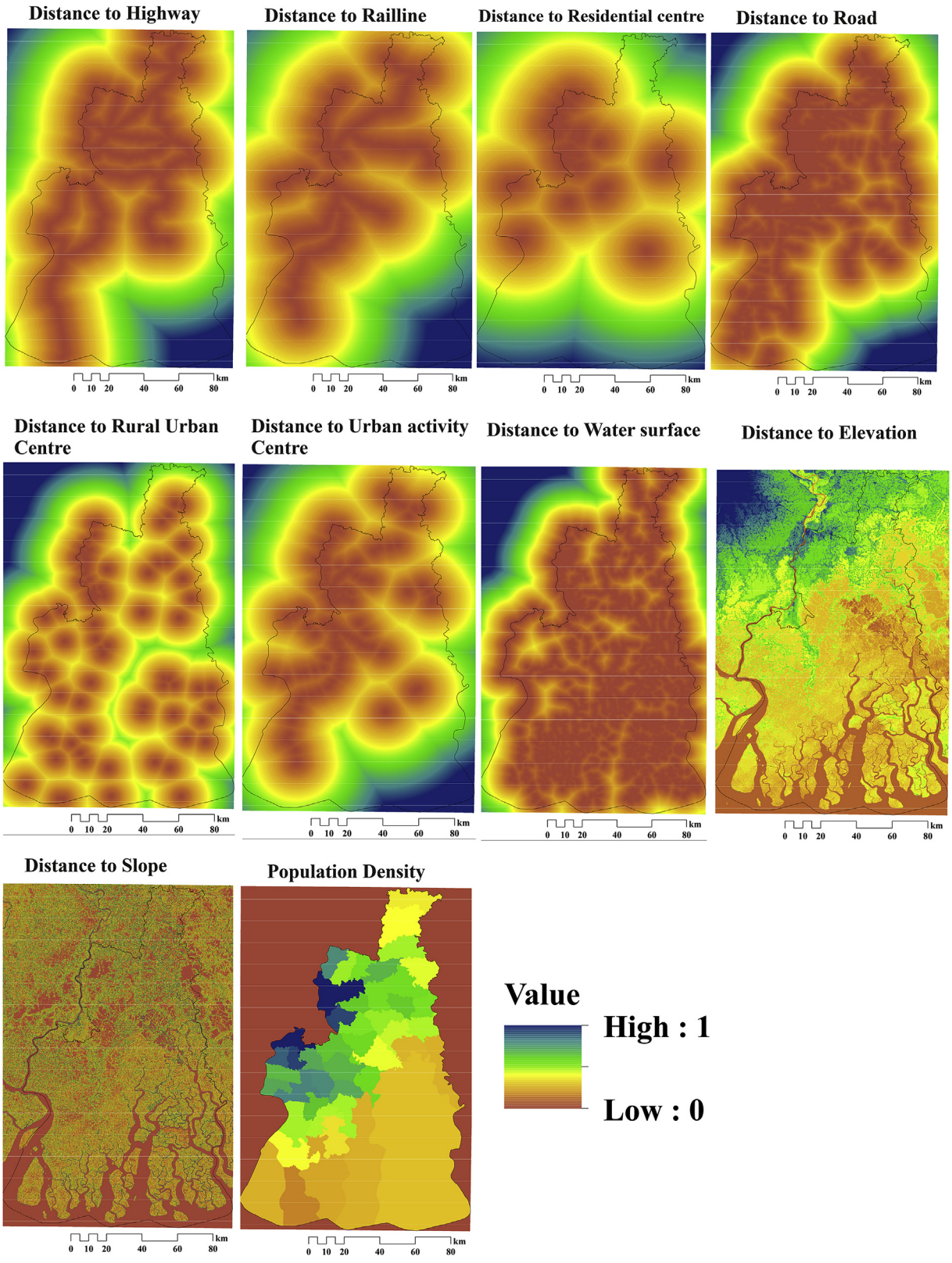

Fig. 8. The fuzzy distance (0–1) estimated for the ten driving factors used in CA-Markov land change model.

mangrove ecosystem, compared to mixed vegetation, and cropland ecosystems (Fig. S8). The annual NPP derived from five NPP models are reported in Table S12. Among the five models, the estimated NPP (gC m^{-2} $year^{-1}$) was maximum for the CASA model, followed by ECLUE, GLO-PEM, MOD17, and VPM model.

The linear association among the NPP models were evaluated and presented in Figs. S9, S10, S11, S12, S13. In 1988, the highest R^2 value was accounted for VPM/ECLUE NPP, followed by MOD17/GLO-PEM, MOD17/ECLUE, GLO-PEM/ECLUE, VPM/GLO-PEM, VPM/MOD17, GLO-PEM/CASA, ECLUE/CASA, VPM/CASA, and MOD17/

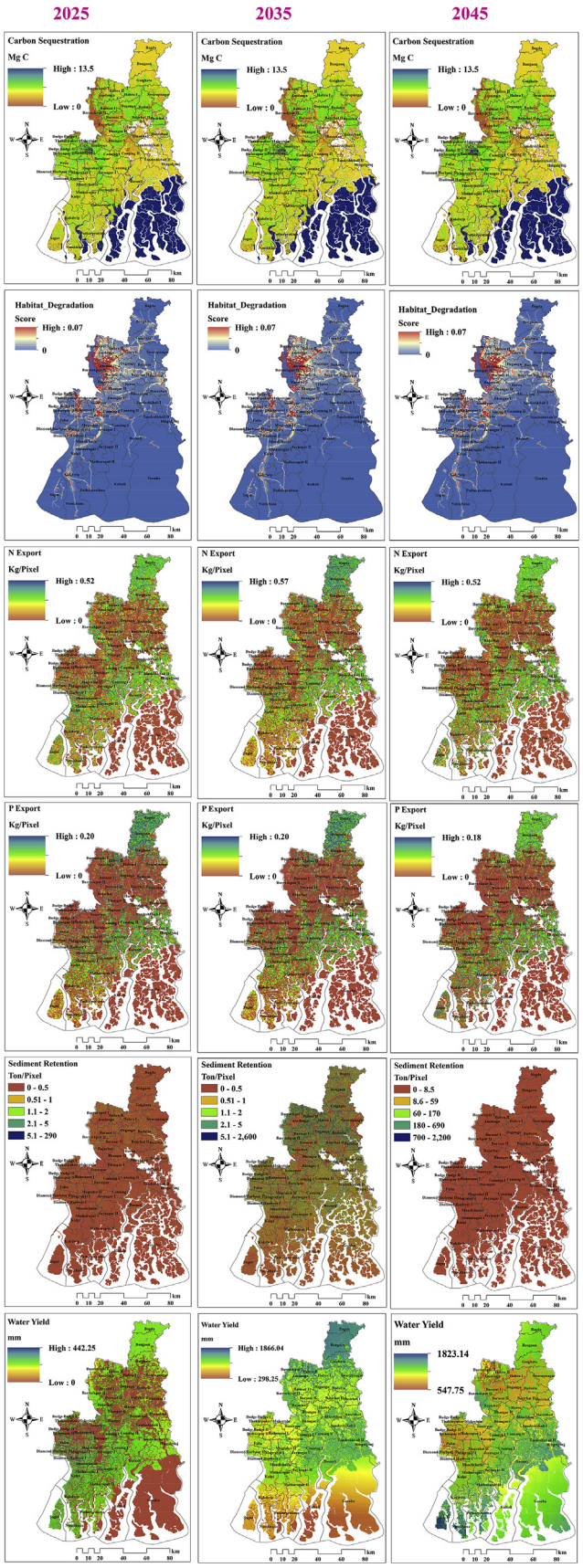

Fig. 9. The biophysical values of different ecosystem services in 2025, 2035, and 2045.

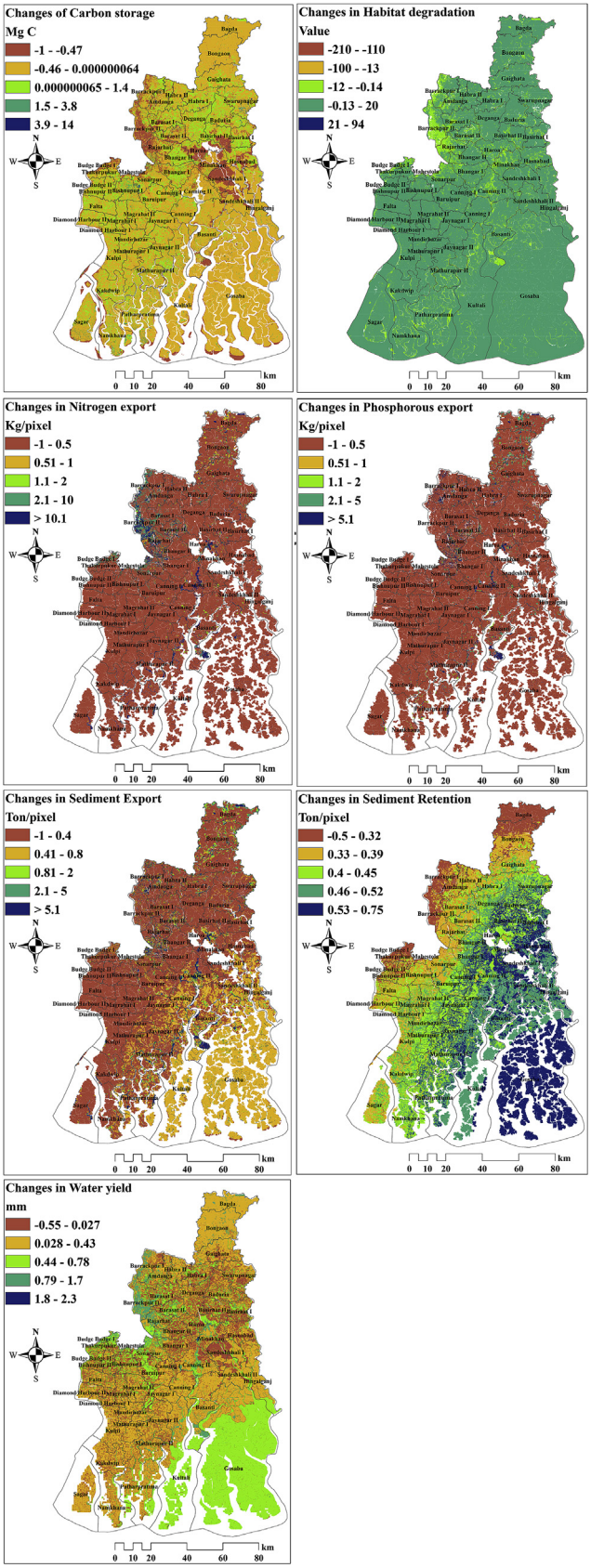

Fig. 10. The spatiotemporal changes of ecosystem services during 1973–2045.

CASA models (Fig. S9). In 2003, the best-paired association was observed between VPM/ECLUE, MOD17/GLOPEM, GLO-PEM/ECLUE, MOD17/ECLUE, VPM/MOD17, VPM/GLO-PEM, MOD17/CASA, GLO-PEM/CASA, ECLUE/CASA, and VPM/CASA NPP (Fig. S10). In 2013, the best model performances were observed between VPM/ECLUE, followed by VPM/MOD17, GLO-PEM/ECLUE, MOD17/ECLUE, VPM/GLO-PEM, MOD17/GLO-PEM, VPM/CASA, ECLUE/CASA, GLO-PEM/CASA, and MOD17/CASA, respectively (Fig. S11). In the last reference year (2017), the high R^2 value was calculated between the VPM/ECLUE, followed by GLO-PEM/ECLUE, VPM/MOD17, MOD17/ECLUE, VPM/GLO-PEM, MOD17/GLO-PEM, VPM/CASA, ECLUE/CASA, GLO-PEM/CASA, and MOD17/CASA NPP (Fig. S12). The spatial association between the NPP models were also evaluated using the Pearson correlation coefficient, and results are reported in Fig. S13. For all five ecosystem models, the high spatial correlation was observed over the mangrove region (Fig. S13).

3.3. Spatiotemporal distribution and changes in ecosystem services

Fig. 2 shows the spatial distribution of ESVs of the key ESs of the Sundarbans region derived from the multiple biophysical models and approaches. Most of these services are highly concentrated over the mangrove region, except for the disturbance regulation service. The maximum per-unit ESVs was estimated for habitat service, nutrient cycling, and gas regulation, whereas, a lower per unit ESVs were approximated for waste treatment, water supply, raw material production services. The biophysical value of key ESs that is derived from the InVEST model is shown in Fig. 3. The carbon sequestration value ranges from 0 to 13.5 MgC per pixel. The total sequestered carbon (MgC) is estimated as 78331769.38, 78521069.19, 79633984.38, 77009844.88, 81684981.32, 82493356.19, 83647453.32, and 84678479.19 in 1973, 1988, 2003, 2013, 2018, 2025, 2035, and 2045, respectively (Table 2). Moreover, due to the expansion of productive natural capitals from 2018 to 2045, the biophysical and economic values of carbon sequestration service will be increased with time. The habitat degradation value ranges from 0 to 0.7, and the maximum habitat degradation and fragmentation is happened in and around the Kolkata city region. This indicates that urbanization can significantly be destabilizing the ecological stability of an ecosystem by fragmentation of natural habitats and the necessary ecosystem services that are essential for sustaining the population and organisms.

The nitrogen export and phosphorous export values (kg $pixel^{-1}$) were found highest over the cropland region, and the minimum values are obtained over the mangrove and wetland ecosystem. The sediment retention service (ton $pixel^{-1}$) is maximum over the cropland and mixed vegetation region, and lowest in wetland and mangrove region. The biophysical values of water yield service (mm) is varied from 429.05 to 2109.57, which is strongly associated with the variability of annual precipitation and evaporation. The maximum water yield values were calculated over the cropland and mixed vegetation region, and the comparatively lower value is being estimated for the mangrove region (Fig. 3). Fig. S14 shows the biophysical values of the nitrogen and phosphorus export and nitrogen and phosphorus load services that were estimated at the watershed level. Among the 13 watersheds of the study region, the maximum values of the said services were obtained at watershed number 66 and 73, which is mostly covered by the mangrove forest. The sediment retention and sediment export services were found high for watershed 66, 72, and 73 (Fig. S14). Noteworthy, the biophysical estimates of the key ESs of Sundarbans derived from the InVEST and CA-Markov models resemble a decline status during 1973–2045 (Figs. S15, S16, S17, S18).

The spatiotemporal changes of the key ESs are evaluated at $P < 0.05$ significance level. To assess the direction (positive and negative) of such changes, the pixel level time series trend test was performed. Except for the habitat and waste treatment services, statistically significant changes were found for the rest of the ESs (Figs. 4 and 5, Fig. S19). The black and white color was showing a statistically significant and insignificant change during (1982–2017), while the positive and negative slope indicates the positive and negative changes of the ESs. Both of these analyses are unveiling the declining status of the ESs in the Sundarbans region. These changes are most prominent over the mangrove region and Kolkata suburban region. The declining status of EVI/NDVI could be aligned with this finding. During the last half of the research period (2000–2017), a sharp decline of the biophysical variables was observed. Among the nine ESs, climate regulation, gas regulation, and disturbance regulation are the most important regulating services of the Sundarbans region. The declining status of these ecosystem services, therefore, unveils a serious socio-economic and livelihood threats to the millions of coastal communities and residents living in this fragile ecosystem.

3.4. Examining the synergy and trade-offs among the ecosystem services

The synergy and tradeoffs of the ESs depend on several factors. These include the nature of the ecosystem services, ecosystem types, scale factors, etc. The synergetic and trade-off among the five ESs is evaluated and reported in Figs. 6 and 7, and Table 3. Among the 21 pairs of ESs, 4 pairs (N_Exp/P_Exp, N_Exp/WY, P_Exp/WY, and Sed_Exp/Sed_Ret) have produced strong positive associations supported by high correlation (r) and regression (R^2) values. Only 3 pairs (C/N_Exp, C/P_Exp, and C/WY) have exhibited a moderate to a weak association, and the rest of the 14 pairs have not produced any obvious correlation. Moreover, among the 21 comparison pairs, 18 of them have created a positive association, and 3 pairs were exhibited a negative correlation; however, all those pairs were statistically significant at $P < 0.05$ (Figs. 6 and 7, Table 3). The carbon sequestration (C) service is found highly correlated (negatively) with the other ESs (Fig. 7). The nutrient cycling service, which is labeled as nitrogen and phosphorous export values in this study, is exhibited a statistically significant positive association with the water yield service. Table 4 shows the positive and negative association between the LULC change driving factors and ESs. Except for the carbon sequestration service, all those explanatory factors have produced a statistically significant negative correlation with the ESs.

3.5. Estimating the future LULC and ecosystem services

The fuzzy distance of the four groups of explanatory factors; i.e. proximity factors (distance to highway, rail line, road), socio-economic and development factors (distance to residential center, rural-urban center, urban activity center), physiographic factors (elevation, slope), and demographic factor (population density) is shown in (Fig. 8). Using the explanatory power of these driving factors, the allocation and changes of future LULC are estimated (Fig. S20). The probability of conversion from mangrove to the coastal estuary and all classes to urban land is evaluated subsequently. Due to the severe threat of sea level rising and resulting in exaggerated coastal erosion, a significant mangrove area would be lost in the coming decades (Fig. S21). Urban sprawl would be evident in and around the Kolkata suburban region at the expense of natural vegetation and cropland (Fig. S22).

The ESs for the future period is calculated from CA-Markov based transitional suitability maps. The biophysical values of five key ESs, i.e., carbon sequestration, habitat degradation, nitrogen export, phosphorous export, sediment retention, and water yield

services were calculated for the three reference years 2025, 2035, and 2045 (Fig. 9). The carbon sequestration service (Mg C) was found maximum over the mangrove and mixed vegetation region. The water bodies, including the coastal estuary and inland wetland, do not have any substantial contribution in sequestrating gaseous carbon from the atmosphere. This could be due to the InVEST and other biophysical approaches employed in this study to quantify the carbon pools, and fluxes merely addressed the terrestrial carbon sequestration, and therefore, the quantitative estimates of the blue carbon pools and fluxes were excluded from the calculation. The future habitat degradation is strongly associated with the process of urbanization and distribution of transport networks (highway, road, rail line) across the region. The nitrogen and phosphorus export services were maximum over the cropland ecosystem, and minimum over the mangrove, mixed vegetation regions.

The spatiotemporal changes of the mentioned services during 1973–2045 is shown in Fig. 10. A slight decrease of carbon sequestration service values is documented over the cropland and mangrove forested region, while such changes were more prominent over the urban region and land which would have converted to the shrimp ponds during the study period. The habitat degradation is apparent, and it is predominantly due to the alteration of cropland and natural vegetation to urban land. Except for the nitrogen and phosphorus export services, the remaining services have shown an incremental trend over the forested mangrove region (Fig. 10). The spatial distribution of the ESs had been evaluated using Moran's I statistics (Figs. S23 and 24). For all reference years, a statistically significant hotspot cluster was observed. These tendencies would be more noticeable in future years (2035, 2045). This suggests that the ESs providing capacity of the natural capitals would be limited to certain areas, and overall ESs delivery capacity of the region would be decreased.

4. Discussion

The performance of the five NPP models was evaluated using the Pearson correlation (r) (both spatial and non-spatial), coefficient of determination (R^2), student's t-test (t) and results suggested that all those models significantly varied across the ecosystems ($P \leq 0.0001$) (Figs. S7, S8, S9, S10, S11, S12, S13). The NPP derived from the said models were also validated with the eddy covariance flux tower data (Rodda et al., 2016). Among the five models, the MOD17 model produced the most consistent estimates, and was thus selected for the subsequent analysis. Fig. S8 revealed that the model performance over the cropland region was not prominent as those obtained for the mangrove and mixed vegetation regions. Biome specific light use efficiency and incomparable environmental stress factors (temperature stress scalar, water stress scalar) that have approximated for each model were probably the principal reasons for varied model performances observed in this study (Yuan et al., 2014; Sannigrahi et al., 2018).

The water stress factor is a crucial limiting factor that predominantly determines model accuracies and uncertainties for both rainfed and moisture deficient ecosystems (Yuan et al., 2014; Wagle et al., 2017). This study adopted multiple approaches to parameterize the water and temperature limiting factors. Like for the calculation of water scalar factor in the CASA model, evaporative function equation (ratio of actual and potential evapotranspiration) was used (Yuan et al., 2015), the energy balance approach (ratio of latent heat and sensible heat) in the GLO-PEM and ECLUE models was used (Prince and Goward, 1995; Yuan et al., 2014). Furthermore, for estimating water stress scalar for VPM and MOD17 models, the remote sensing-based band rationing and vapor pressure deficit function was utilized (Zhang et al., 2016). Likewise, several discrete methods were approximated to evaluate the temperature stress effects on potential light use efficiency and photosynthesis. These structural differences might be responsible for the model differences observed in this study.

The biophysical and economic values of the key ESs were calculated for both time-series (1982–2017) and individual years (1973, 1988, 2003, 2013, 2018, 2025, 2035, 2045) (Figs. 2–5). The highest ESVs (US$ ha^{-1}) was estimated for habitat service (30780), nutrient cycling (12626), and gas regulation (7224.81), whereas, lower values of ESV were approximated for water regulation (347.81), raw material production (777.82) and waste treatment (13.57) services. Since two different approaches were adopted: *biophysical approach*, which is entirely based on the calculation of NPP, and *model-based approach*, which is connected to InVEST and CA-Markov based modeling, it has found that most of these services evaluated in this study were highly sensitive to the changes of EVI/NDVI and LULC (Carreño et al., 2012; Yu and Han, 2016; Zhang et al., 2017). Furthermore, the spatial trend and slope estimation suggested a significant decline in the key ESs of the Sundarbans region. This pixel-level estimation provides more intuitive pictures about the status of ESs than that of any conventional non-spatial estimates. However, this invites uncertainties as the visual quality of the pixel is highly affected by atmospheric conditions and chances of getting erroneous pixel reflectance would be high if proper preprocessing was deployed prior to the final analysis. The declining status of the ESs is more prominent during the second phase of the research period (2000–2017). The key biophysical variables (EVI, NDVI, fPAR), which were used as inputs for estimating the time-series NPP and ESs, were found decreasing during 2000–2017. These findings could be aligned with the degradation of ESs in the Sundarbans.

Among the popular approaches, such as benefit transfer method (Costanza et al., 2014; 2014), biophysical modelling and mapping (Nelson et al., 2009), contingent valuation (Carson, 2000), statistical value transfer (de Groot et al., 2012), travel cost (Mayer and Woltering, 2018), replacement cost (Förster et al., 2019), hedonic methods (Sander and Haight, 2012), available for estimating the valuation and mapping of ESs, only the biophysical modeling and spatially explicit integrated modeling approaches were incorporated in this study to calculate the economic and biophysical values of multiple key ESs of Sundarbans. The biophysical approaches were mainly used for the calculation of economic values of the ESs, while the spatially explicit models integrated with InVEST and CA-Markov produced the biophysical values of the services. According to Nelson et al. (2009), the spatially explicit tools like InVEST is highly effective as it can perform at any levels of complication and produced the biophysical and monetary values simultaneously, depending on the requirements of decision-makers and concerned stakeholders. However, this turns the model sensitive to a specific condition like data availability and variation of system dynamics (Nelson et al., 2009).

The degradation of natural capitals can be significantly affected by the ESs provision by altering the structure, process, functions of an ecosystem (Chen et al., 2019). Among the six primary ESs that were derived from the InVEST biophysical model, one ES (carbon capture) entirely depends on the fluctuation of LULC inputs. This summarily designates that any form of land management policies and land reform strategies that encourage the conversion of productive land, especially the highly productive mangrove forest, for the development or any other financial benefits, will be disrupted the ideal man-nature balance of this ecosystem. The rest of the ESs including the nitrogen and phosphorous export, sediment retention, and water yield services are connected to both climatic and land-use dynamics, and thus, make them more sensitive and vulnerable to any unwanted modification. The dissemination of

productive lands will entirely govern the future ESs provision and spatial distribution. This also resonates the need for preserving valuable natural capitals, which provide the essential goods, services, and functions to the betterment of human welfare and overall societal well-being. Additionally, it is required to integrate different valuation approaches in order to assess environmental well-being and social-ecological impacts under changing climate and land degradation and to better understand the amplification effect – synergic and trade-off interactions of drivers that could intensify the causal effects on ESs or offset effects – changes in one driver can modulate the effect of another driver on ESs.

5. Conclusion

Using both biophysical and spatially explicit integrated models, this study evaluated and quantified biophysical and monetary values of key ecosystem services in the Sundarbans biosphere region, India. Quantification was made both in time series (1982–2017) and individual years (1973, 1988, 2003, 2013, 2018, 2025, 2035, 2045) to understand the long-term ecological status of the region. The key biophysical variables including EVI, NDVI fPAR, NPP revealed a decremental state during the research period, especially in the western part of the Sundarbans and Kolkata suburban region. The fast-tracked urbanization especially over Kolkata and its surrounding region, the disappearance of mangroves due to severe coastal erosion, and the increasing salinity especially the western part of the region, could be associated with the declining status of EVI, NDVI, and NPP observed in this study. Among the nine ecosystem services evaluated in this study, climate regulation, gas regulation, and disturbance regulation are the most important regulating services of the Sundarbans region. The declining status of these ecosystem services, therefore, unveils a serious socio-economic and livelihood threats to the millions of coastal communities and residents living in this fragile ecosystem. The outcomes of this study could provide an important reference to the land administrators, researchers, and decision-makers to comprehend the expected human-nature juxtaposition in protected natural reserve regions like the Sundarbans. Therefore, the generic approaches and methods proposed in this study have the potential of resolving the problems encountered by the decision-makers in local and regional scale policy formulation. The ESs chosen in this study is highly relevant to the ecosystems and ecology of the Sundarbans. However, several other ESs, whose biophysical and economic significance were not evaluated here but should be evaluated and reported, will be cover with some future studies. Several other factors are also responsible for the degradation of ecosystem services.

Declaration of competing interest

The authors whose names are listed in this manuscript certify that they have NO affiliations with or involvement in any organization or entity with any financial interest or non-financial interest in the subject matter or materials discussed in this manuscript.

CRediT authorship contribution statement

Srikanta Sannigrahi: Conceptualization, Formal analysis, Writing - original draft, Writing - review & editing. **Qi Zhang:** Visualization, Writing - review & editing. **P.K. Joshi:** Writing - review & editing, Supervision. **Paul C. Sutton:** Investigation, Methodology, Writing - review & editing. **Saskia Keesstra:** Writing - review & editing, Supervision. **P.S. Roy:** Conceptualization, Investigation, Supervision, Writing - review & editing. **Francesco Pilla:** Supervision, Writing - review & editing. **Bidroha Basu:** Writing - review & editing. **Ying Wang:** Visualization, Writing - review & editing. **Shouvik Jha:** Formal analysis, Investigation, Visualization. **Saikat Kumar Paul:** Conceptualization, Supervision. **Somnath Sen:** Conceptualization, Supervision.

Acknowledgment

The authors express their sincere gratitude to the anonymous reviewers and the Editorial Board for fruitful and constructive comments to enhance the quality of the paper. SS acknowledge University Grants Commission (UGC) for providing continuous research fellowship to carry out the research at Indian Institute of Technology (IIT), Kharagpur, India.

Appendix A. Supplementary data

Supplementary data to this article can be found online at https://doi.org/10.1016/j.jclepro.2020.120424.

References

Anselin, L., 1995. Local indicators of spatial association—LISA. Geogr. Anal. 27 (2), 93–115.
Barral, M.P., Oscar, M.N., 2012. Land-use planning based on ecosystem service assessment: a case study in the Southeast Pampas of Argentina. Agric. Ecosyst. Environ. 154, 34–43. https://doi.org/10.1016/j.agee.2011.07.010.
Bennett, E.M., Peterson, G.D., Gordon, L.J., 2009. Understanding relationships among multiple ecosystem services. Ecol. Lett. 12 (12), 1394–1404.
Blumstein, M., Thompson, J.R., 2015. Land-use impacts on the quantity and configuration of ecosystem service provisioning in Massachusetts, USA. J. Appl. Ecol. 52 (4), 1009–1019.
Braat, L.C., de Groot, R., 2012. The ecosystem services agenda: bridging the worlds of natural science and economics, conservation and development, and public and private policy. Ecosyst. Serv. 1 (1), 4–15. https://doi.org/10.1016/j.ecoser.2012.07.011.
Burkhard, B., Kroll, F., Müller, F., Windhorst, W., 2009. Landscapes' capacities to provide ecosystem services-a concept for land-cover based assessments. Landscape online 15, 1–22.
Burkhard, B., Kandziora, M., Hou, Y., Müller, F., 2014. Ecosystem service potentials, flows and demands-concepts for spatial localisation, indication and quantification. Landscape online 34, 1–32.
Cabral, P., Feger, C., Levrel, H., Chambolle, M., Basque, D., 2016. Assessing the Impact of Land-Cover Changes on Ecosystem Services : A Fi Rst Step toward Integrative Planning in Bordeaux , France. Ecosystem Services, pp. 318–327. https://doi.org/10.1016/j.ecoser.2016.08.005 (in press).
Cademus, R., Escobedo, F.J., McLaughlin, D., Abd-Elrahman, A., 2014. Analyzing trade-offs, synergies, and drivers among timber production, carbon sequestration, and water yield in Pinus elliotii forests in southeastern USA. Forests 5 (6), 1409–1431.
Carreño, L., Frank, F.C., Viglizzo, E.F., 2012. Tradeoffs between economic and ecosystem services in Argentina during 50 years of land-use change. Agric. Ecosyst. Environ. 154, 68–77. https://doi.org/10.1016/j.agee.2011.05.019.
Carson, R.T., 2000. Contingent Valuation: A user's guide. Environ. Sci. Technol. 34 (8), 1413–1418. https://doi.org/10.1021/es990728j.
Cerretelli, S., Poggio, L., Gimona, A., Yakob, G., Boke, S., Habte, M., et al., 2018. Spatial assessment of land degradation through key ecosystem services: the role of globally available data. Sci. Total Environ. 628–629, 539–555. https://doi.org/10.1016/j.scitotenv.2018.02.085.
Chen, W., Chi, G., Li, J., 2019. Science of the Total Environment the spatial association of ecosystem services with land use and land cover change at the county level in China , 1995 – 2015. Sci. Total Environ. 669, 459–470. https://doi.org/10.1016/j.scitotenv.2019.03.139.
Chen, Y., Li, X., Liu, X., Zhang, Y., Huang, M., 2019. Tele-connecting China's future urban growth to impacts on ecosystem services under the shared socioeconomic pathways. Sci. Total Environ. 652, 765–779. https://doi.org/10.1016/j.scitotenv.2018.10.283.
Clerici, N., Cote-Navarro, F., Escobedo, F.J., Rubiano, K., Villegas, J.C., 2019. Spatio-temporal and cumulative effects of land use-land cover and climate change on two ecosystem services in the Colombian Andes. Sci. Total Environ. 685, 1181–1192. https://doi.org/10.1016/j.scitotenv.2019.06.275.
Costanza, R., 2012. Ecosystem health and ecological engineering. Ecol. Eng. 45, 24–29. https://doi.org/10.1016/j.ecoleng.2012.03.023.
Costanza, R., De Groot, R., Sutton, P., Van der Ploeg, S., Anderson, S.J., Kubiszewski, I., et al., 2014. Changes in the global value of ecosystem services. Global Environ. Change 26, 152–158.
Costanza, R., De Groot, R., Braat, L., Kubiszewski, I., Fioramonti, L., Sutton, P., et al., 2017. Twenty years of ecosystem services: how far have we come and how far do we still need to go? Ecosyst. Serv. 28, 1–16.

Crabtree, R., Potter, C., Mullen, R., Sheldon, J., Huang, S., Harmsen, J., et al., 2009. A modeling and spatio-temporal analysis framework for monitoring environmental change using NPP as an ecosystem indicator. Rem. Sens. Environ. 113 (7), 1486–1496. https://doi.org/10.1016/j.rse.2008.12.014.

Cramer, W., Kicklighter, D.W., Bondeau, a, Moore, B., Churkina, G., Nemry, B., et al., 1999. Comparing global models of terrestrial net primary productivity (NPP): overview and key results. Global Change Biol. 5, 1–15. https://doi.org/10.1046/j.1365-2486.1999.00001.x.

DasGupta, R., Hashimoto, S., Okuro, T., Basu, M., 2019. Scenario-based land change modelling in the Indian Sundarban delta: an exploratory analysis of plausible alternative regional futures. Sustain. Sci. 14 (1), 221–240. https://doi.org/10.1007/s11625-018-0642-6.

DeFries, R.S., Field, C.B., Fung, I., Collatz, G.J., Bounoua, L., 1999. Combining satellite data and biogeochemical models to estimate global effects of human-induced land cover change on carbon emissions and primary productivity. Global Biogeochem. Cycles 13 (3), 803–815. https://doi.org/10.1029/1999GB900037.

Dwyer, J., Roy, D., Sauer, B., Jenkerson, C., Zhang, H., Lymburner, L., 2018. Analysis ready data: enabling analysis of the Landsat archive. Rem. Sens. 10 (9), 1363. https://doi.org/10.3390/rs10091363.

Everard, M., Kangabam, R., Tiwari, M.K., McInnes, R., Kumar, R., Talukdar, G.H., et al., 2019. Ecosystem service assessment of selected wetlands of Kolkata and the Indian Gangetic Delta: multi-beneficial systems under differentiated management stress. Wetl. Ecol. Manag. 27 (2–3), 405–426. https://doi.org/10.1007/s11273-019-09668-1.

Fan, C., Myint, S., 2014. A comparison of spatial autocorrelation indices and landscape metrics in measuring urban landscape fragmentation. Landsc. Urban Plann. 121, 117–128.

Fang, J., Song, H., Zhang, Y., Li, Y., Liu, J., 2018. Climate-dependence of ecosystem services in a nature reserve in northern China. PloS One 13 (2), 1–17. https://doi.org/10.1371/journal.pone.0192727.

Fang, X., Zhu, Q., Ren, L., Chen, H., Wang, K., Peng, C., 2018. Large-scale detection of vegetation dynamics and their potential drivers using MODIS images and BFAST: a case study in Quebec, Canada. Rem. Sens. Environ. 206, 391–402. https://doi.org/10.1016/j.rse.2017.11.017. March 2016.

Förster, J., Schmidt, S., Bartkowski, B., Lienhoop, N., Albert, C., Wittmer, H., 2019. Incorporating environmental costs of ecosystem service loss in political decision making: a synthesis of monetary values for Germany. PloS One 14 (2), e0211419. https://doi.org/10.1371/journal.pone.0211419. Retrieved from.

Fu, W.J., Jiang, P.K., Zhou, G.M., Zhao, K.L., 2014. Using Moran's I and GIS to study the spatial pattern of forest litter carbon density in a subtropical region of southeastern China. Biogeosciences 11 (8), 2401–2409.

García-Palomares, J.C., Gutiérrez, J., Mínguez, C., 2015. Identification of tourist hot spots based on social networks: a comparative analysis of European metropolises using photo-sharing services and GIS. Appl. Geogr. 63, 408–417.

Giri, C., Ochieng, E., Tieszen, L.L., Zhu, Z., Singh, A., Loveland, T., et al., 2011. Status and distribution of mangrove forests of the world using earth observation satellite data. Global Ecol. Biogeogr. 20 (1), 154–159.

Groot, R., Brander, L., van der Ploeg, S., Costanza, R., Bernard, F., Braat, L., van Beukering, P., 2012. Global estimates of the value of ecosystems and their services in monetary units. Ecosyst. Serv. 1 (1), 50–61. https://doi.org/10.1016/j.ecoser.2012.07.005.

Guo, Z., Xiao, X., Gan, Y., Zheng, Y., 2001. Ecosystem functions, services and their values - a case study in Xingsham country of China. Ecol. Econ. 38, 141–154. https://doi.org/10.1016/S0921-8009(01)00154-9.

Haase, D., Schwarz, N., Strohbach, M., Kroll, F., Seppelt, R., 2012. Synergies, trade-offs, and losses of ecosystem services in urban regions: an integrated multiscale framework applied to the Leipzig-Halle Region, Germany. Ecol. Soc. 17 (3).

Harries, K., 2006. Extreme spatial variations in crime density in Baltimore County, MD. Geoforum 37, 404–406.

Hauck, J., Görg, C., Varjopuro, R., Ratamäki, O., Jax, K., 2013. Benefits and limitations of the ecosystem services concept in environmental policy and decision making: some stakeholder perspectives. Environ. Sci. Pol. 25, 13–21. https://doi.org/10.1016/j.envsci.2012.08.001.

Hou, H., Wang, R., Murayama, Y., 2019. Scenario-based modelling for urban sustainability focusing on changes in cropland under rapid urbanization: a case study of Hangzhou from 1990 to 2035. Sci. Total Environ. 661, 422–431. https://doi.org/10.1016/j.scitotenv.2019.01.208.

Hu, Y., Peng, J., Liu, Y., Tian, L., 2018. Integrating ecosystem services trade-offs with paddy land-to-dry land decisions: a scenario approach in Erhai Lake Basin, southwest China. Sci. Total Environ. 625, 849–860. https://doi.org/10.1016/j.scitotenv.2017.12.340.

Jacquin, A., Sheeren, D., Lacombe, J.P., 2010. Vegetation cover degradation assessment in Madagascar savanna based on trend analysis of MODIS NDVI time series. Int. J. Appl. Earth Obs. Geoinf. 12 (Suppl. 1), 3–10. https://doi.org/10.1016/j.jag.2009.11.004.

Jiang, C., Li, D., Wang, D., Zhang, L., 2016. Quantification and assessment of changes in ecosystem service in the Three-River Headwaters Region, China as a result of climate variability and land cover change. Ecol. Indicat. 66, 199–211. https://doi.org/10.1016/j.ecolind.2016.01.051.

Johnston, R.J., Russell, M., 2011. An operational structure for clarity in ecosystem service values. Ecol. Econ. 70 (12), 2243–2249. https://doi.org/10.1016/j.ecolecon.2011.07.003.

Kibria, A.S.M.G., Behie, A., Costanza, R., Groves, C., Farrell, T., 2017. The value of ecosystem services obtained from the protected forest of Cambodia: the case of Veun Sai-Siem Pang National Park. Ecosyst. Serv. 26, 27–36. https://doi.org/10.1016/j.ecoser.2017.05.008.

Krause, S., Jacobs, J., Voss, A., Bronstert, A., Zehe, E., 2008. Assessing the impact of changes in landuse and management practices on the diffuse pollution and retention of nitrate in a riparian floodplain. Sci. Total Environ. 389 (1), 149–164.

Lang, Y., Song, W., Zhang, Y., 2017. Responses of the water-yield ecosystem service to climate and land use change in Sancha River Basin, China. Phys. Chem. Earth 101, 102–111. https://doi.org/10.1016/j.pce.2017.06.003.

Langerwisch, F., Václavík, T., von Bloh, W., Vetter, T., Thonicke, K., 2017. Combined effects of climate and land-use change on the provision of ecosystem services in rice agro-ecosystems. Environ. Res. Lett. 13 (1), 015003 https://doi.org/10.1088/1748-9326/aa954d.

Lee, J.H., Heo, J.H., 2011. Evaluation of estimation methods for rainfall erosivity based on annual precipitation in Korea. J. Hydrol. 409 (1–2), 30–48.

Leroux, L., Bégué, a., Lo Seen, D., Jolivot, a., Kayitakire, F., 2016. Driving forces of recent vegetation changes in the Sahel: lessons learned from regional and local level analyses. Rem. Sens. Environ. 191, 38–54. https://doi.org/10.1016/j.rse.2017.01.014.

Levine, N., 2004. The CrimeStat Program: Characteristics, Use and Audience. Geographical Analysis, Forthcoming.

Li, S., 2012. Vegetation regrowth trends in post forest fire ecosystems across North America from 2000 to 2010. Nat. Sci. (10), 755–770. https://doi.org/10.4236/ns.2012.410100, 04.

Li, B., Wang, W., 2018. Trade-offs and synergies in ecosystem services for the Yinchuan Basin in China. Ecol. Indicat. 84, 837–846.

Li, B., Chen, N., Wang, Y., Wang, W., 2018. Spatio-temporal quantification of the trade-offs and synergies among ecosystem services based on grid-cells: a case study of Guanzhong Basin, NW China. Ecol. Indicat. 94, 246–253. https://doi.org/10.1016/j.ecolind.2018.06.069. June.

Liang, Y., Liu, L., Huang, J., 2017. Integrating the SD-CLUE-S and InVEST models into assessment of oasis carbon storage in northwestern China. PloS One 12 (2), e0172494. https://doi.org/10.1371/journal.pone.0172494.

Liu, C., Xu, Y., Huang, A., Li, Y., Wang, H., Lu, L., et al., 2018. Spatial identification of land use multifunctionality at grid scale in farming-pastoral area: a case study of Zhangjiakou City, China. Habitat Int. 76, 48–61. https://doi.org/10.1016/j.habitatint.2018.05.010.

Liu, C., Zhang, Q., Luo, H., Qi, S., Tao, S., Xu, H., Yao, Y., 2019a. An efficient approach to capture continuous impervious surface dynamics using spatial-temporal rules and dense Landsat time series stacks. Rem. Sens. Environ. 229, 114–132. https://doi.org/10.1016/j.rse.2019.04.025.

Liu, Y., Lü, Y., Fu, B., Harris, P., Wu, L., 2019b. Quantifying the spatio-temporal drivers of planned vegetation restoration on ecosystem services at a regional scale. Sci. Total Environ. 650, 1029–1040. https://doi.org/10.1016/j.scitotenv.2018.09.082.

Lü, Y., Fu, B., Feng, X., Zeng, Y., Liu, Y., Chang, R., et al., 2012. A policy-driven large scale ecological restoration: quantifying ecosystem services changes in the Loess Plateau of China. PloS One 7 (2), e31782. https://doi.org/10.1371/journal.pone.0031782.

Luo, Y., Lü, Y., Fu, B., Zhang, Q., Li, T., Hu, W., Comber, A., 2018. Half century change of interactions among ecosystem services driven by ecological restoration: quantification and policy implications at a watershed scale in the Chinese Loess Plateau. Sci. Total Environ. 651, 2546–2557. https://doi.org/10.1016/j.scitotenv.2018.10.116.

Millennium Ecosystem Assessment (Ma), 2005. Ecosystems and Human Well-Being: Synthesis. Island Press, Washington DC.

Marx, A., Erhard, M., Thober, S., Kumar, R., Schäfer, D., Samaniego, L., Zink, M., 2019. Climate change as driver for ecosystem services risk and opportunities. In: Atlas of Ecosystem Services. Springer, Cham, pp. 173–178.

Mayer, M., Woltering, M., 2018. Assessing and valuing the recreational ecosystem services of Germany's national parks using travel cost models. Ecosyst. Serv. 31, 371–386. https://doi.org/10.1016/j.ecoser.2017.12.009.

Nandy, S., Kushwaha, S.P.S., 2011. Study on the utility of IRS 1D LISS-III data and the classification techniques for mapping of Sunderban mangroves. J. Coast Conserv. 15 (1), 123–137. https://doi.org/10.1007/s11852-010-0126-z.

Nelson, E., Mendoza, G., Regetz, J., Polasky, S., Tallis, H., Cameron, D., et al., 2009. Modeling multiple ecosystem services, biodiversity conservation, commodity production, and tradeoffs at landscape scales. Front. Ecol. Environ. 7 (1), 4–11.

Pandeya, B., Buytaert, W., Zulkafli, Z., Karpouzoglou, T., Mao, F., Hannah, D.M., 2016. A comparative analysis of ecosystem services valuation approaches for application at the local scale and in data scarce regions. Ecosyst. Serv. 22, 250–259. https://doi.org/10.1016/j.ecoser.2016.10.015. November 2015.

Peng, J., Liu, Y., Wu, J., Lv, H., Hu, X., 2015. Linking ecosystem services and landscape patterns to assess urban ecosystem health: a case study in Shenzhen City, China. Landsc. Urban Plann. 143, 56–68. https://doi.org/10.1016/j.landurbplan.2015.06.007.

Potter, C.S., Randerson, J.T., Field, C.B., Matson, P.A., Vitousek, P.M., Mooney, H.A., Klooster, S.A., 1993. Terrestrial ecosystem production: a process model based on global satellite and surface data. Global Biogeochem. Cycles 7 (4), 811–841. https://doi.org/10.1029/93GB02725.

Prince, S.D., Goward, S.N., 1995. Global primary production: a remote sensing approach. J. Biogeogr. 815–835.

Qiu, S., Lin, Y., Shang, R., Zhang, J., Ma, L., Zhu, Z., 2019. Making Landsat time series consistent: evaluating and improving Landsat analysis ready data. Rem. Sens. 11 (1), 51. https://doi.org/10.3390/rs11010051.

Rahman, M., Asaduzzaman, M., 2013. Ecology of Sundarban, Bangladesh. J. Sci. Found. 8 (1–2), 35–47. https://doi.org/10.3329/jsf.v8i1-2.14618.

Ray, R., Majumder, N., Das, S., Chowdhury, C., Jana, T.K., 2014. Biogeochemical cycle

of nitrogen in a tropical mangrove ecosystem , east coast of India. Mar. Chem. 167, 33–43. https://doi.org/10.1016/j.marchem.2014.04.007.
Ray, R., Rixen, T., Baum, A., Malik, A., Gleixner, G., Jana, T.K., 2015. Estuarine , Coastal and Shelf Science Distribution , sources and biogeochemistry of organic matter in a mangrove dominated estuarine system (Indian Sundarbans) during the pre-monsoon. Estuar. Coast Shelf Sci. 167, 404–413. https://doi.org/10.1016/j.ecss.2015.10.017.
Ray, R., Majumder, N., Chowdhury, C., Das, S., Jana, T.K., 2018. Phosphorus budget of the Sundarban mangrove ecosystem: box model approach. Estuar. Coast 41 (4), 1036–1049. https://doi.org/10.1007/s12237-017-0332-0.
Redhead, J.W., Stratford, C., Sharps, K., Jones, L., Ziv, G., Clarke, D., et al., 2016. Empirical validation of the InVEST water yield ecosystem service model at a national scale. Sci. Total Environ. 569, 1418–1426.
Renard, K.G., Freimund, J.R., 1994. Using Monthly Precipitation Data to Estimate the R-Factor in the Revised USLE.
Ricke, K., Drouet, L., Caldeira, K., Tavoni, M., 2018. Country-level social cost of carbon. Nat. Clim. Change 8 (10), 895–900. https://doi.org/10.1038/s41558-018-0282-y.
Rodda, S.R., Thumaty, K.C., Jha, C.S., Dadhwal, V.K., 2016. Seasonal variations of carbon dioxide, water vapor and energy fluxes in tropical Indian mangroves. Forests 7 (2), 35.
Rodríguez, J.P., Beard Jr., T.D., Bennett, E.M., Cumming, G.S., Cork, S.J., Agard, J., et al., 2006. Trade-offs across space, time, and ecosystem services. Ecol. Soc. 11 (1).
Ruimy, a., Kergoat, L., Bondeau, a., 1999. Comparing global models of terrestrial net primary productivity (NPP): analysis of differences in light absorption and light-use efficiency. Global Change Biol. 5 (Suppl. 1), 56–64. https://doi.org/10.1046/j.1365-2486.1999.00007.x.
Rukundo, E., Liu, S., Dong, Y., Rutebuka, E., Asamoah, E.F., Xu, J., Wu, X., 2018. Spatio-temporal dynamics of critical ecosystem services in response to agricultural expansion in Rwanda, East Africa. Ecol. Indicat. 89 (February), 696–705. https://doi.org/10.1016/j.ecolind.2018.02.032.
Running, S.W., Nemani, R.R., Heinsch, F.A., Zhao, M., Reeves, M., Hashimoto, H., 2004. A continuous satellite-derived measure of global terrestrial primary production. Bioscience 54 (6), 547–560.
Sahle, M., Saito, O., Fürst, C., Demissew, S., Yeshitela, K., 2019. Future land use management effects on ecosystem services under different scenarios in the Wabe River catchment of Gurage Mountain chain landscape, Ethiopia. Sustain. Sci. 14 (1), 175–190. https://doi.org/10.1007/s11625-018-0585-y.
Sander, H.A., Haight, R.G., 2012. Estimating the economic value of cultural ecosystem services in an urbanizing area using hedonic pricing. J. Environ. Manag. 113, 194–205. https://doi.org/10.1016/j.jenvman.2012.08.031.
Sannigrahi, S., Bhatt, S., Rahmat, S., Paul, S.K., Sen, S., 2018. Estimating global ecosystem service values and its response to land surface dynamics during 1995–2015. J. Environ. Manag. 223, 115–131. https://doi.org/10.1016/j.jenvman.2018.05.091.
Sannigrahi, S., Chakraborti, S., Joshi, P.K., Keesstra, S., Sen, S., Paul, S.K., Dang, K.B., 2019a. Ecosystem service value assessment of a natural reserve region for strengthening protection and conservation. J. Environ. Manag. 244, 208–227. https://doi.org/10.1016/j.jenvman.2019.04.095.
Sannigrahi, S., Joshi, P.K., Keesstra, S., Paul, S.K., Sen, S., Roy, P.S., Bhatt, S., 2019b. Evaluating landscape capacity to provide spatially explicit valued ecosystem services for sustainable coastal resource management. Ocean Coast Manag. 182, 104918. https://doi.org/10.1016/j.ocecoaman.2019.104918.
Sannigrahi, S., Zhang, Q., Pilla, F., Joshi, P.K., Basu, B., Keesstra, S., Roy, P.S., Wang, Y., Sutton, P.C., Chakraborti, S., Paul, S.K., Sen, S., 2020. Responses of ecosystem services to natural and anthropogenic forcings: a spatial regression based assessment in the world's largest mangrove ecosystem. Sci. Total Environ. 715, 137004 https://doi.org/10.1016/j.scitotenv.2020.137004.
Seixas, J., Carvalhais, N., Nunes, C., Benali, a., 2009. Comparative analysis of MODIS-FAPAR and MERIS-MGVI datasets: potential impacts on ecosystem modeling. Rem. Sens. Environ. 113 (12), 2547–2559. https://doi.org/10.1016/j.rse.2009.07.018.
Sharp, R., Tallis, H.T., Ricketts, T., Guerry, A.D., Wood, S.A., Chaplin-Kramer, R., et al., 2018. InVEST 3.4. 4 User's Guide. The Natural Capital Project.
Sil, Â., Fonseca, F., Gonçalves, J., Honrado, J., Marta-Pedroso, C., Alonso, J., et al., 2017. Analysing carbon sequestration and storage dynamics in a changing mountain landscape in Portugal: insights for management and planning. Int. J. Biodiv. Sci., Ecosyst. Serv. & Manag. 13 (2), 82–104. https://doi.org/10.1080/21513732.2017.1297331.
Song, W., Deng, X., Yuan, Y., Wang, Z., Li, Z., 2015a. Impacts of land-use change on valued ecosystem service in rapidly urbanized North China Plain. Ecol. Model. https://doi.org/10.1016/j.ecolmodel.2015.01.029.
Song, W., Deng, X., Yuan, Y., Wang, Z., Li, Z., 2015b. Impacts of land-use change on valued ecosystem service in rapidly urbanized North China Plain. Ecol. Model. 318, 245–253. https://doi.org/10.1016/j.ecolmodel.2015.01.029.
Storey, J., Choate, M., Lee, K., 2014. Landsat 8 operational land imager on-orbit geometric calibration and performance. Rem. Sens. 6 (11), 11127–11152. https://doi.org/10.3390/rs61111127.
Su, C., Fu, B., Wei, Y., Lü, Y., Liu, G., Wang, D., et al., 2012. Ecosystem management based on ecosystem services and human activities: a case study in the Yanhe watershed. Sustain. Sci. 7, 17–32. https://doi.org/10.1007/s11625-011-0145-1.
Sun, C., Wang, S., Zou, W., 2016. Chinese marine ecosystem services value: regional and structural equilibrium analysis. Ocean Coast Manag. 125, 70–83. https://doi.org/10.1016/j.ocecoaman.2016.03.001.
Tallis, H.T., Ricketts, T., Guerry, A.D., Nelson, E., Ennaanay, D., Wolny, S., et al., 2011. InVEST 2.1 Beta User's Guide. Integrated Valuation of Ecosystem Services and Tradeoffs.
Tomscha, S.A., Gergel, S.E., 2016. Ecosystem service trade-offs and synergies misunderstood without landscape history. Ecol. Soc. 21 (1).
Trajkovic, S., 2007. Hargreaves versus Penman-Monteith under humid conditions. J. Irrigat. Drain. Eng. 133 (1), 38–42. https://doi.org/10.1061/(ASCE)0733-9437(2007)133:1(38).
Valipour, M., 2015. Temperature analysis of reference evapotranspiration models. Meteorol. Appl. 22 (3), 385–394. https://doi.org/10.1002/met.1465.
Verbesselt, J., Hyndman, R., Newnham, G., Culvenor, D., 2010. Detecting trend and seasonal changes in satellite image time series. Rem. Sens. Environ. 114 (1), 106–115. https://doi.org/10.1016/j.rse.2009.08.014.
Wagle, P., Gowda, P.H., Anapalli, S.S., Reddy, K.N., Northup, B.K., 2017. Growing season variability in carbon dioxide exchange of irrigated and rainfed soybean in the southern United States. Sci. Total Environ. 593, 263–273.
Wang, X., Chen, W., Zhang, L., Jin, D., Lu, C., 2010. Estimating the ecosystem service losses from proposed land reclamation projects: a case study in Xiamen. Ecol. Econ. 69 (12), 2549–2556. https://doi.org/10.1016/j.ecolecon.2010.07.031.
Wang, J., Dong, J., Liu, J., Huang, M., Li, G., Running, S.W., et al., 2014. Comparison of gross primary productivity derived from GIMMS NDVI3g, GIMMS, and MODIS in Southeast Asia. Rem. Sens. 6 (3), 2108–2133.
Wang, Y., Li, X., Zhang, Q., Li, J., Zhou, X., 2018. Projections of future land use changes: multiple scenarios-based impacts analysis on ecosystem services for Wuhan city, China. Ecol. Indicat. 94, 430–445. https://doi.org/10.1016/j.ecolind.2018.06.047.
Wang, Y., Bilsborrow, R.E., Zhang, Q., Li, J., Song, C., 2019. Effects of payment for ecosystem services and agricultural subsidy programs on rural household land use decisions in China: synergy or trade-off? Land Use Pol. 81, 785–801. https://doi.org/10.1016/j.landusepol.2018.10.057.
Watson, S.C.L., Paterson, D.M., Queirós, A.M., Rees, A.P., Stephens, N., Widdicombe, S., Beaumont, N.J., 2016. A conceptual framework for assessing the ecosystem service of waste remediation : in the marine environment. Ecosyst. Serv. 20, 69–81. https://doi.org/10.1016/j.ecoser.2016.06.011.
Watson, K.B., Galford, G.L., Sonter, L.J., Koh, I., Ricketts, T.H., 2019. Effects of human demand on conservation planning for biodiversity and ecosystem services. Conserv. Biol. https://doi.org/10.1111/cobi.13276.
Wu, X., Liu, S., Zhao, S., Hou, X., Xu, J., Dong, S., Liu, G., 2019. Quantification and driving force analysis of ecosystem services supply, demand and balance in China. Sci. Total Environ. 652, 1375–1386. https://doi.org/10.1016/j.scitotenv.2018.10.329.
Xiao, X., Zhang, Q., Braswell, B., Urbanski, S., Boles, S., Wofsy, S., et al., 2004. Modeling gross primary production of temperate deciduous broadleaf forest using satellite images and climate data. Rem. Sens. Environ. 91 (2), 256–270.
Xiao, Y., Xie, G., Lu, C., Ding, X., Lu, Y., 2005. The value of gas exchange as a service by rice paddies in suburban Shanghai, PR China. Agric. Ecosyst. Environ. 109 (3–4), 273–283. https://doi.org/10.1016/j.agee.2005.03.016.
Xie, X., Li, A., Jin, H., Tan, J., Wang, C., Lei, G., et al., 2019. Assessment of five satellite-derived LAI datasets for GPP estimations through ecosystem models. Sci. Total Environ. 690, 1120–1130. https://doi.org/10.1016/j.scitotenv.2019.06.516.
Xu, X., Yang, G., Tan, Y., Liu, J., Hu, H., 2018. Ecosystem services trade-offs and determinants in China's Yangtze river economic belt from 2000 to 2015. Sci. Total Environ. 634, 1601–1614. https://doi.org/10.1016/j.scitotenv.2018.04.046.
Yan, Y., Zhao, C., Wang, C., Shan, P., Zhang, Y., Wu, G., 2016. Ecosystem health assessment of the Liao River Basin upstream region based on ecosystem services. Acta Ecol. Sin. 36 (4), 294–300. https://doi.org/10.1016/j.chnaes.2016.06.005.
Yang, S., Zhao, W., Liu, Y., Wang, S., Wang, J., Zhai, R., 2018. Influence of land use change on the ecosystem service trade-offs in the ecological restoration area: dynamics and scenarios in the Yanhe watershed, China. Sci. Total Environ. 644 (19), 556–566. https://doi.org/10.1016/j.scitotenv.2018.06.348.
Yu, D., Han, S., 2016. Ecosystem service status and changes of degraded natural reserves–A study from the Changbai Mountain Natural Reserve, China. Ecosyst. Serv. 20, 56–65. https://doi.org/10.1016/j.ecoser.2016.06.009.
Yuan, W., Liu, S., Zhou, G., Zhou, G., Tieszen, L.L., Baldocchi, D., et al., 2007. Deriving a light use efficiency model from eddy covariance flux data for predicting daily gross primary production across biomes. Agric. For. Meteorol. 143 (3–4), 189–207.
Yuan, W., Cai, W., Xia, J., Chen, J., Liu, S., Dong, W., et al., 2014. Agricultural and Forest Meteorology Global comparison of light use efficiency models for simulating terrestrial vegetation gross primary production based on the LaThuile database. Agric. For. Meteorol. 192–193, 108–120. https://doi.org/10.1016/j.agrformet.2014.03.007.
Yuan, W., Cai, W., Nguy-Robertson, A.L., Fang, H., Suyker, A.E., Chen, Y., Zhang, H., 2015. Uncertainty in simulating gross primary production of cropland ecosystem from satellite-based models. Agric. For. Meteorol. 207, 48–57. https://doi.org/10.1016/j.agrformet.2015.03.016.
Zhang, L., Dawes, W.R., Walker, G.R., 2001. Response of mean annual evapotranspiration to vegetation changes at catchment scale. Water Resour. Res. 37 (3), 701–708.
Zhang, C., Luo, L., Xu, W., Ledwith, V., 2008. Use of local Moran's I and GIS to identify pollution hotspots of Pb in urban soils of Galway, Ireland. Sci. Total Environ. 398 (1–3), 212–221.
Zhang, L.X., Zhou, D.C., Fan, J.W., Hu, Z.M., 2015. Comparison of four light use efficiency models for estimating terrestrial gross primary production. Ecol. Model. 300, 30–39. https://doi.org/10.1016/j.ecolmodel.2015.01.001.

Zhang, Y., Zhang, C., Wang, Z., Chen, Y., Gang, C., An, R., Li, J., 2016. Vegetation dynamics and its driving forces from climate change and human activities in the Three-River Source Region, China from 1982 to 2012. Sci. Total Environ. 563, 210–220.

Zhang, L., Lü, Y., Fu, B., Dong, Z., Zeng, Y., Wu, B., 2017. Mapping ecosystem services for China ' s ecoregions with a biophysical surrogate approach. Landsc. Urban Plann. 161, 22–31. https://doi.org/10.1016/j.landurbplan.2016.12.015.

Zhang, Q., Song, C., Chen, X., 2018. Effects of China's payment for ecosystem services programs on cropland abandonment: a case study in Tiantangzhai Township, Anhui, China. Land Use Pol. 73, 239–248. https://doi.org/10.1016/j.landusepol.2018.01.001.

Zhang, Q., Bilsborrow, R.E., Song, C., Tao, S., Huang, Q., 2019. Rural household income distribution and inequality in China: effects of payments for ecosystem services policies and other factors. Ecol. Econ. 160, 114–127. https://doi.org/10.1016/j.ecolecon.2019.02.019.

Zoderer, B.M., Stanghellini, P.S.L., Tasser, E., Walde, J., Wieser, H., Tappeiner, U., 2016. Exploring socio-cultural values of ecosystem service categories in the Central Alps: the influence of socio-demographic factors and landscape type. Reg. Environ. Change 16 (7), 2033–2044. https://doi.org/10.1007/s10113-015-0922-y.